Development and performance analysis of an object-oriented model for phase change material thermal storage

Michael Jokiel

Project Work

June 2016 – July 2016

Department of Thermal Energy

SINTEF Energy Research

SINTEF

Abstract

On the basis of the energy system installed at the University College of Bergen (Høgskolen i Bergen) the general fundamentals of thermal energy storage (TES) are presented. In particular, the advantages of TES that consist of phase change materials (PCM) are discussed.

Building climate control systems are facing dynamic boundary conditions like a changing ambient temperature or varying cooling loads inside the building. TES can be implemented in the systems to correct the gap between supply and demand and to improve the performance and reliability of the thermal system. Surplus energy could be saved and re-used in case of heating or cooling shortages. PCMs are a promising type of an efficient TES. During a constant-temperature process a high amount of latent heat of fusion can be released or absorbed.

Based on these conditions, a dynamic model for a PCM energy storage is developed. The utilized equations and derived relations are illustrated, followed by an explanation of the required input data. The TES model was written in object-oriented Modelica code. The model was implemented into an existing model library and validated with different sets of measurement data from both the plant in Bergen and the PCM manufacturer.

The performance of the TES of the University College in Bergen was examined and assessed in comparison to provided manufacturer's performance data sheets and preliminary design calculations. The report ends with a conclusion and proposals for further work.

SINTEF

Content

SINTEF

List of Figures

SINTEF

List of Tables

List of Symbols and Abbreviations

Greek Letters

α	Heat Transfer Coefficient	$\mathrm{W\,m^{-2}\,K^{-1}}$
β	Thermal Expansion Coefficient	$\mathrm{K^{-1}}$
λ	Thermal Conductivity	$\mathrm{W\,m^{-1}}\,K^{-1}$
ρ	Density	$\mathrm{kg\,m^{-3}}$
η	Dynamic Viscosity	$\mathrm{kg\,m^{-1}}\,s^{-1}$
v	Kinematic Viscosity	$\mathrm{m^2\,s^{-1}}$

Roman Letters

A	Cross-Sectional Area	$\mathrm{m^2}$
b	Flow Channel Width	m
b	PCM Storage Tank Width	m
c_p	Specific Heat Capacity (p const.)	$\mathrm{kJ\,kg^{-1}\,K^{-1}}$
d	PCM Container Wall Thickness	m
h	Flow Channel Height	m
h	PCM Storage Tank Height	m
h	Specific Enthalpy	$\mathrm{kJ\,kg^{-1}}$
k	Factor	
l	Flow Channel Length	m
l	PCM Storage Tank Length	m
m	Mass	kg
$\dot{m}$	Mass Flow Rate	$\mathrm{kg\,s^{-1}}$
n	Number, Amount	$\mathrm{s^{-1}}$
n	Discretization	
Nu	Nusselt-Number	
Q	Integrated Heat Flow Rate, Energy	
$\dot{Q}$	Heat Flow Rate, Cooling Capacity	W
p	Pressure	bar
Pr	Prandtl-Number	$\mathrm{kg\,m\,s^{-1}}$
R	Thermal Resistance	$\mathrm{m\,K\,W^{-1}}$
Ra	Rayleigh-Number	
Re	Reynolds-Number	
t	Time	s
T	Temperature	K
v	Specific Volume	$\mathrm{m^3\,kg^{-1}}$
v	Relative Fluid Velocity	$\mathrm{m\,s^{-1}}$
$\dot{V}$	Volume Flow	$\mathrm{m^3\,s^{-1}}$
x	Liquid Mass Fraction	

Subscripts

$cells$	Discretization
$containers$	Related to PCM Containers
$flow\ channel$	Related to the Gap Between PCM Containers
in	At Inlet
$init$	Value for Initialization
NS	In the Direction of the Heat Flow
out	At Outlet
$port$	Related to the Heat Port of the Cell
$tank$	Related to PCM Storage Tank
$wall$	Related to PCM Container Wall
WE	In the Direction Perpendicular to the Heat Flow

Abbreviations

HDPE	High-Density Polyethylene
HX	Heat Exchanger
PCM	Phase Change Material
SLE	Solid-Liquid Equilibrium
TES	Thermal Energy Storage

1 Introduction

Buildings account for 37 % of the energy use in the EU (Perez-Lombard 2008). In order to reduce the energy demand and the climate gas emissions, the energy efficiency in buildings has to be improved. In non-residential buildings, such as offices and educational buildings, substantial amounts of waste heat are often available due to the high cooling demand. Thus, energy systems for such buildings should be designed to avoid heat disposal. This has been the design principle for the energy system at the University College in Bergen (Dar 2014). The system employs different types of thermal energy storages (TES) – energy wells and phase change materials (PCM) – to transfer and to store surplus heat to utilize it upon demand. This report focuses on modelling and analysis of the PCM storage system.

Models of storage systems and simulations of their performance are required to be able to make assumptions and predictions on the design, dimensioning and layout of storage units. Real world test rigs can be cost intensive and especially time intensive, since the storage of thermal energy is connected to rather slow and inert processes. With the help of a model the dynamic behaviour of the system can be examined for several boundary conditions.

Chapter 2 provides detailed information about the TES that is utilized at the University College in Bergen. The motivation of using PCM as a TES is discussed.

After the basics about the implementation of TES are given, chapter 3 presents a derivation of a model for a PCM thermal energy storage. The required information about the utilized equations and the needed input parameters are explained.

Chapter 4 includes the validation results of the modelled TES. For this sake real world measurement data is used, taken from the construction in Bergen and the PCM manufacturer. Additionally, the performance of the installed PCM storage system in Bergen is evaluated and comparisons to the assumptions that were applied at the design phase are made. In particular charging and discharging dynamics of the PCM storage are examined.

The last chapter summarizes the conclusions that were drawn from the analysis. The presented results increase the understanding of the PCM storage and should provide a base for improved implementation of such a storage in future systems. Finally, deficits of the current model are presented and activities for further work are proposed.

2 Basics

2.1 Thermal Energy Storage

An energy storage provides the ability to capture energy produced at a point of time for later utilization. Energy is available in different forms, such as thermal, chemical, electrical, potential and kinetic. The energy storage often involves converting energy from forms that are difficult to store to more conveniently storable forms. Figure 1 presents the different types for energy storages.

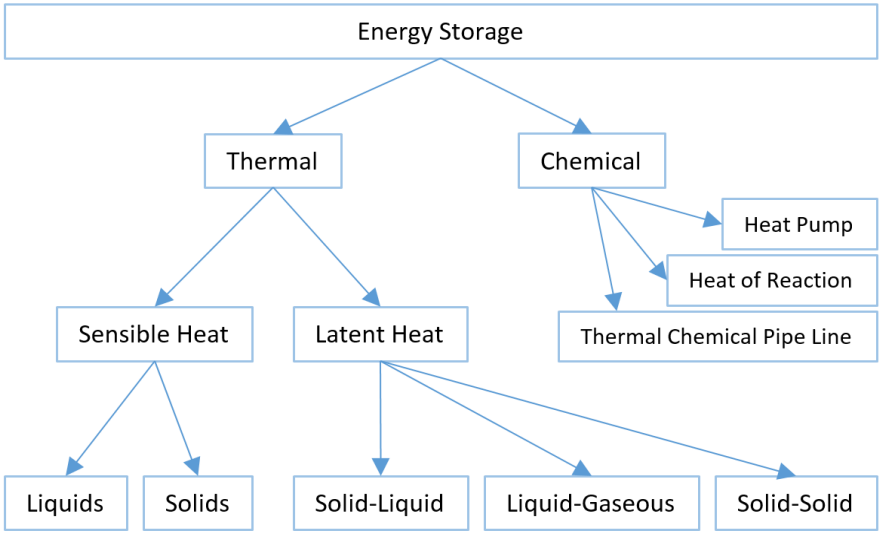

Figure 1 – Types of energy storage (Sharma 2007, modified)

Thermal energy storage (TES) has been recognized as one of the most efficient ways to enhance the energy efficiency and sustainability of heating and cooling systems (Liu 2016). Storing high or low temperature energy for a later use can bridge the time gap between energy availability and energy use. That way the use of TES in building applications can improve the indoor thermal comfort, reduce machinery size, decrease running cost, improve the system reliability and therefore enhance the total energy efficiency.

Thermal energy can be stored in PCMs. Due to their high latent heat during phase change processes large amounts of energy can be stored in relatively small volumes. The stored energy can be retrieved when the process is reversed. Figure 2 illustrates that heating and cooling the material occurs without a temperature change during the actual phase change. Therefore an energy flow to the PCM can be provided even if only small temperature differences between the PCM and the heat transfer fluid are available.

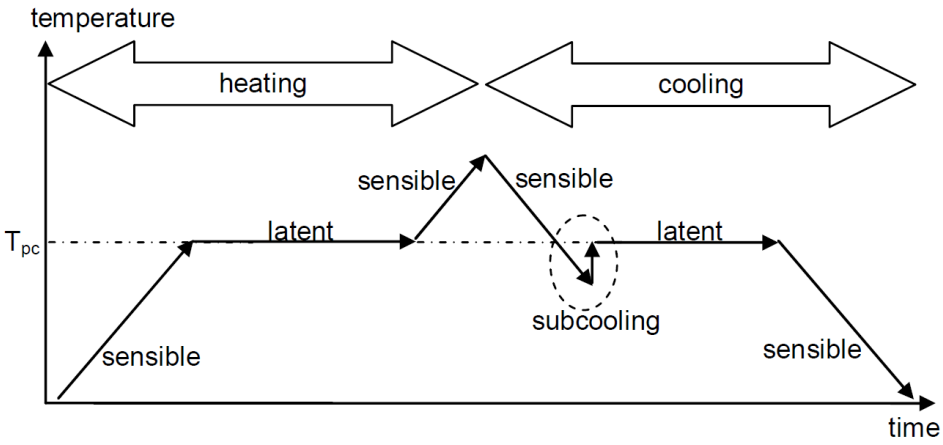

Figure 2 – Schematic cycle for melting and freezing of a PCM (Mehling 2008)

A subcooling effect results from nucleation processes during the beginning of the PCM freezing. It is dependent on the type of the PCM, just as the particular freezing and melting temperature. The choice of a proper PCM with a suitable freezing/melting temperature is dependent on the overall cooling system and can be customized for any application.

The following section gives a small overview of the energy system at the University College in Bergen. Furthermore the procedure for implementing a PCM thermal energy storage system in the energy system will be discussed.

2.2 PCM Thermal Energy Storage at University College Bergen

This section gives a brief explanation on how to implement a TES into an energy system. For this sake the energy system of the University College of Bergen will be displayed, which features four PCM cold storage tanks (see figure 3) in its chilled water distribution loop.

Figure 3 – PCM cold storage tanks of University College Bergen (Dar2014)

These tanks are filled with small containers that contain PCM. The salt hydrate in these containers has a phase change temperature of 10 °C (PCM Products Ltd. 2011). Water flows through the tanks and through the small flow passage between the stacked PCM containers.

The educational building of the University College of Bergen has a total area of over 50,000 m^2 and was projected for an annual heating demand of 2600 MWh and a cooling demand of 1060 MWh. Its peak heating and cooling loads are 2830 kW and 3000 kW, respectively (Dar 2014). The installed cooling capacity is higher than the heating demand, due to the high amount of excess heat during summer months due to solar radiation and high internal loads from students, computers, servers, IT rooms, etc.

To maintain the thermal comfort of the building on an appropriate level the room temperature needs to stay at minimum 18 °C (Uno 2007), despite a fluctuating ambient temperature and varying internal loads. An implemented TES has a compensating effect that enables the system to react to transient peak ambient temperatures without increasing the power consumption of the heat pump system. Figure 4 illustrates the potential of decreasing the machinery size of the cooling system after an implementation of a thermal storage at the energy system of the University College in Bergen.

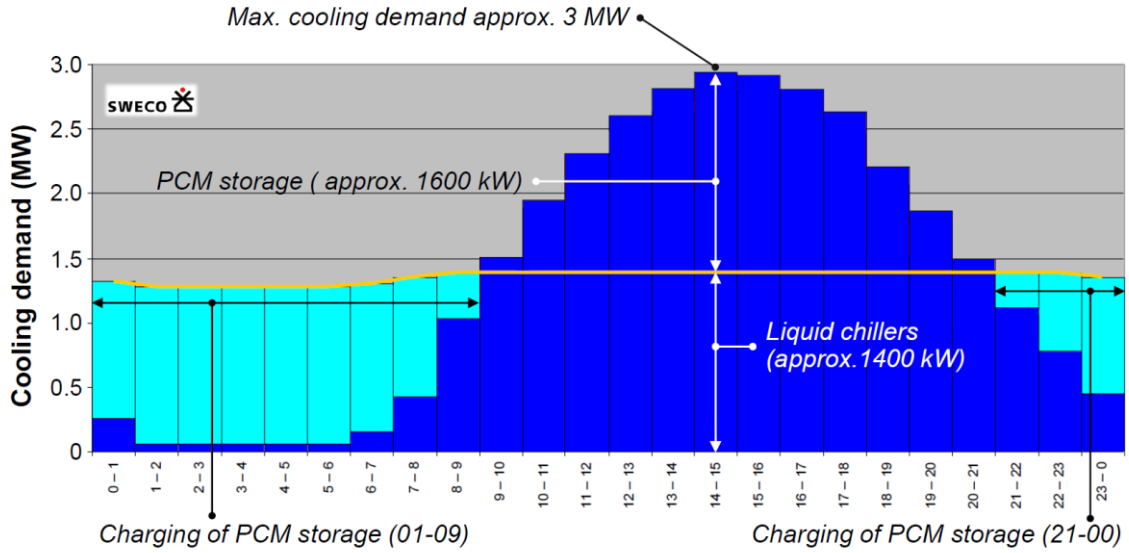

Figure 4 – Cooling demand over the daytime at University College Bergen (Sweco 2014, modified)

The utilized liquid chillers are providing an averaged capacity of only 1400 kW over the whole daytime, although the peak load of the cooling demand is 3000 kW. Furthermore, the cooling demand during the night-time is drastically reduced. Thus, a thermal storage unit can utilize this discrepancy and save the cooling capacity at night to release it on demand during

the day. Thus, there is no necessity to design the liquid chillers to cover the peak load, which leads to smaller machinery size and thus lower operating costs.

To optimize investment costs and to minimize operational costs, the heating and cooling production system combines an ammonia heat pump/chiller installation with thermal energy storages: a ground-source TES for seasonal energy storage and four PCM accumulation tanks to provide peak load cooling and backup cooling capacity (Dar 2014). Thus, the PCM tanks are used as daily energy storage. A simplified scheme of the integrated thermal energy system can be seen in figure 5.

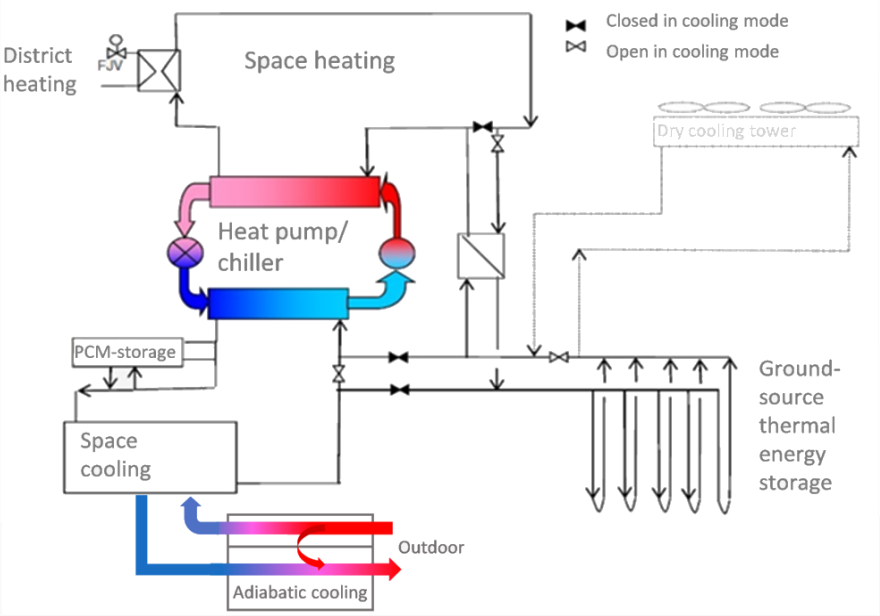

Figure 5 – Simplified scheme of the energy system at University College Bergen (Dar 2014)

The report focuses on the performance evaluation of the PCM cold storage and the chilled water distribution loop. Therefore only the cooling performance of the energy system will be evaluated, leaving aside the heating system, the adiabatic cooling system and the ground source TES. A simplified scheme of the evaluated subsystem is shown in figure 6.

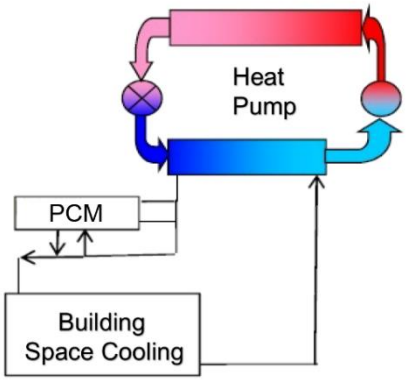

Figure 6 – Simplified scheme of the chilled water distribution loop (Dar 2014, modified)

The PCM cold storage tanks are positioned in the chilled water distribution loop. Four tanks with a total volume of 228 m^3 (single tank volume 57 m^3) and a total storage capacity of 11,240 kWh (single tank capacity 2810 kWh) are implemented in the energy system, rendering the PCM storage system the largest of its kind in Europe. The PCM storage enabled a ~50 % reduction in the installed chiller cooling capacity resulting in reduced operational costs for the energy system. Furthermore, an investment cost reduction was obtained, mainly due to the reduction in the installed chiller cooling capacity and the number of boreholes (Dar 2014).

Figure 7 shows a detailed system scheme for the chilled water loop, implementing the PCM storage tanks into the energy system of the University College in Bergen.

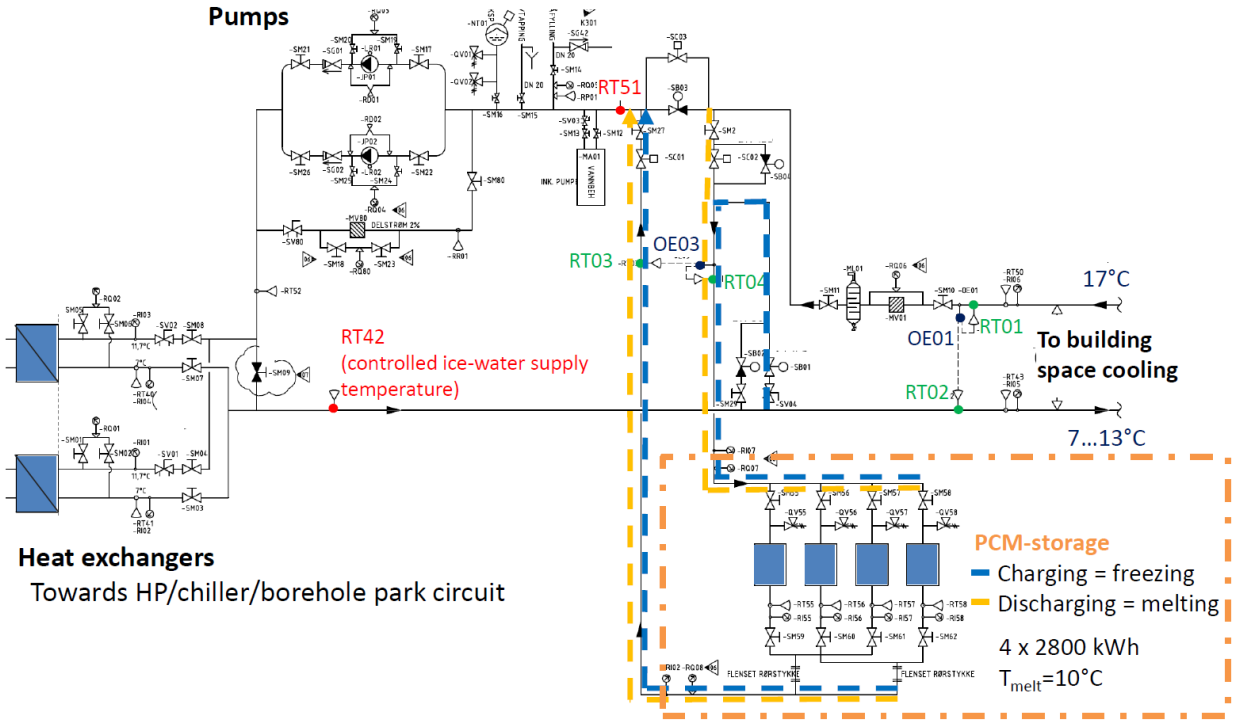

Figure 7 – Detailed system scheme of the chilled water distribution loop at University College Bergen (Dar 2014)

The model derived in chapter 3 will simply consist of the PCM tank and inlet and outlet boundaries for the water (orange rectangle in figure 7). The blue and yellow dashed lines in figure 7 mark the flow directions for water, corresponding to different operation modes for the PCM storage tanks. When the PCM tanks are not in use, the equivalent bypass valves are closed and no mass flow occurs at the energy meter OE03. The purpose of the chilled water loop is to provide water for space cooling at a supply temperature of 7 – 13 °C at an

inlet/return temperature of approximately 17 $°C$. In case the PCM tanks are used, two different operation modes can be distinguished:

The mass flow direction marked with blue in figure 7 represents the operation mode of charging or freezing of the PCM. In this mode, the bypass valves allow a mass flow of chilled water into the PCM tanks. The mass flow is supplied from the supply/inlet side of the space cooling unit, resulting in a reduced cooling capacity that can be provided to the building. The charging operation mode will be usually initiated if the inlet water temperature (sensor RT02) reaches a very low level of $< 7\ °C$ or if the cooling demand of the building is generally on a reduced level, for example at night-time operation.

The mass flow direction marked with yellow in figure 7 displays the operation mode of discharging or melting the PCM. In this case the PCM storages are fed by heated water from the space cooling return/outlet side, for example in case of return water temperatures of $> 17\ °C$ (sensor RT01). Without the cooling effect of a discharging PCM storage, the overheated water would result in an increased power demand in the heat pump/chiller unit.

Hence, with a proper application of the charging and discharging ability of the PCM storage tanks, surplus cooling capacity can be used (in the form of freezing the PCM) to compensate peak cooling demands (in the form of melting the PCM), leading to an increased overall efficiency of the cooling system.

Precise knowledge about the dynamic charging and discharging behaviour of the PCM storage is fundamental for designing and dimensioning a storage system. Models and simulations can provide new information and understanding about the storage performance. Consequently, the next chapter discusses an approach for modelling a PCM thermal storage.

3 The Heat Exchanger Model for a PCM Thermal Storage

In this chapter the general approach for modelling a PCM thermal energy storage system will be discussed. The PCM storage model has been implemented using already existing Modelica libraries for thermal fluid systems. "TIL" is a model library for thermal components and systems, while "TIL Media" contains a model library including thermophysical properties for the utilized fluids (Frohböse 2015). These libraries were provided by TLK-Thermo GmbH, a German company for simulation technology and software development.

The aim with the Modelica model is to be able to investigate the charging and discharging dynamics and hence to increase the understanding of the PCM storage. That way the model could provide a best practice data sheet and a base for a more optimal implementation of future systems.

3.1 Derivation

The first challenge in modelling a TES consisting of PCM is to find suitable equations and relations to express the real world behaviour of the storage. Since a thermal storage is basically just exchanging heat with the chilled water distribution loop, a suitable approach for a model is to use a simple heat exchanger (HX) model and modify and extend it to represent a PCM cold storage. A derivation for this modification and extension will be given in this section.

The utilized PCM storage tank from the University College of Bergen is filled with smaller PCM containers that are stacked inside the tank, as shown in figure 8 (a). The water flows in between these containers. Figure 8 (b) shows a typical heat transfer model, which served as a general starting point for the present PCM storage model.

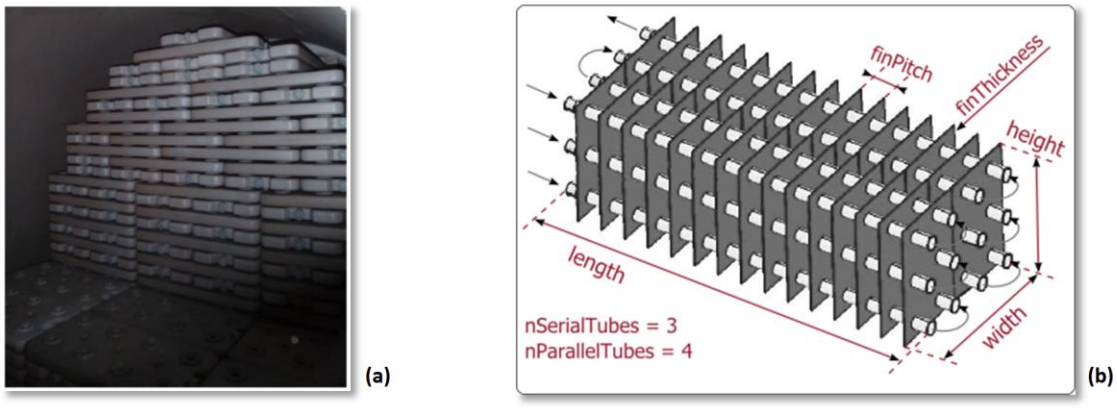

Figure 8 – Derivation of the model: PCM containers in a PCM storage tank (a) (Dar 2014), typical heat exchanger used for most HX models (b) (TIL Library)

The actual PCM storage is cylindrical. However, for simplification, a rectangular model was applied. Figure 9 illustrates the steps of transforming the stacked PCM containers in a cylindrical tank to a setup that resembles an ordinary rectangular HX structure.

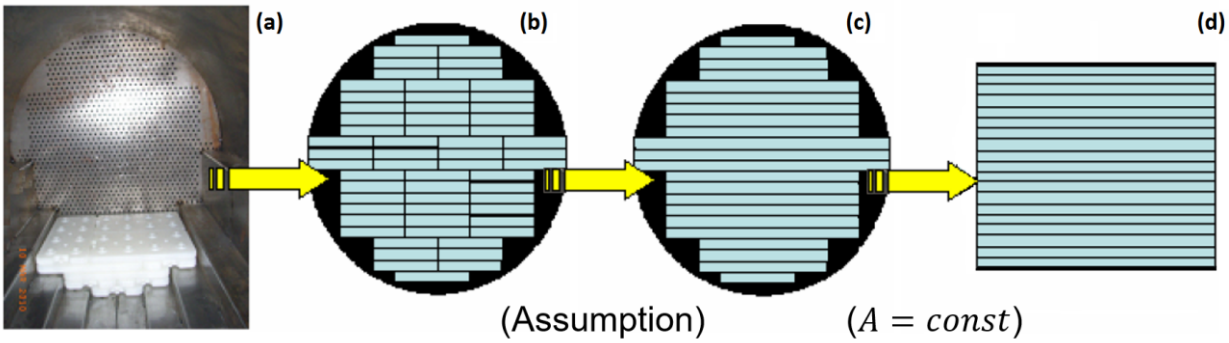

Figure 9 – Derivation of the model: Transforming stacked PCM containers to a rectangular flow channel structure (PCM Products Ltd. 2011, modified)

After the PCM containers are stacked in a compact way inside the tank, a cross-sectional area as shown in figure 9b is formed. Figure 9c assumes that the walls between individual containers that are arranged side by side can be neglected. Hence, the formerly tubes of the ordinary HX model from figure 8b are now the gaps between the containers, resulting in very wide, flat and narrow water flow channels. Finally, figure 9d is derived by transforming the formerly round shape of the tank into a square one while the cross-sectional area of the tank is kept constant. A square cross-sectional flow area will be easier to manage in regard to mass flow and heat transfer calculations.

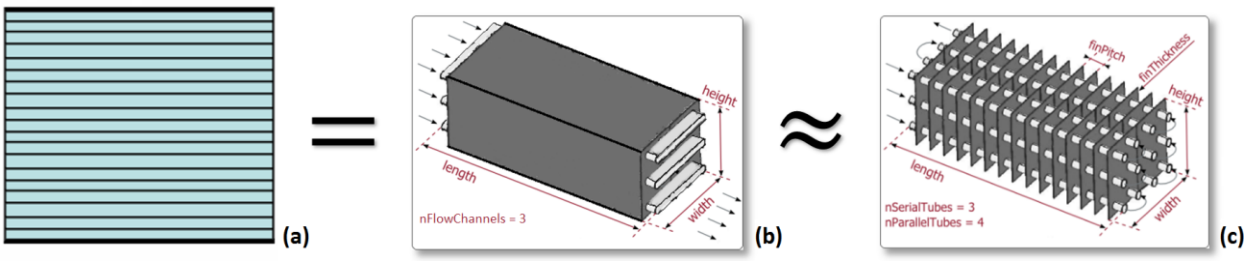

Figure 10 – Derivation of the model: New flow channel structure resembles initial heat exchanger

Figure 10 summarizes the geometric derivation of the model. The newly derived HX model in figure 10b resembles an ordinary HX model. To apply an existing HX model for the PCM tank, the following assumptions need to be made:

- Flat rectangular flow ducts are used within the HX instead of ordinary round pipes.
- The walls of the flow channels are the walls of the PCM containers.

- A mass flow is only existent on the water side. The PCM side of the HX is a closed system with a constant mass of PCM.
- The mass flow of water occurs in one direction. There is no occurrence of backflow or recirculation flow within the PCM tank.
- No additional geometries like fins are used in the PCM heat exchanger. The heat transfer occurs only between the boundaries of "water to container wall" and "container wall to PCM".

The following section provides further information about the composition and parametrization of the modified HX model.

3.2 General Layout

This chapter gives a detailed overview of the model's general structure and its parametrization. The layout of the HX model will be illustrated and exemplary estimations for the input parameters are given. Figure 11 shows the setup of the model.

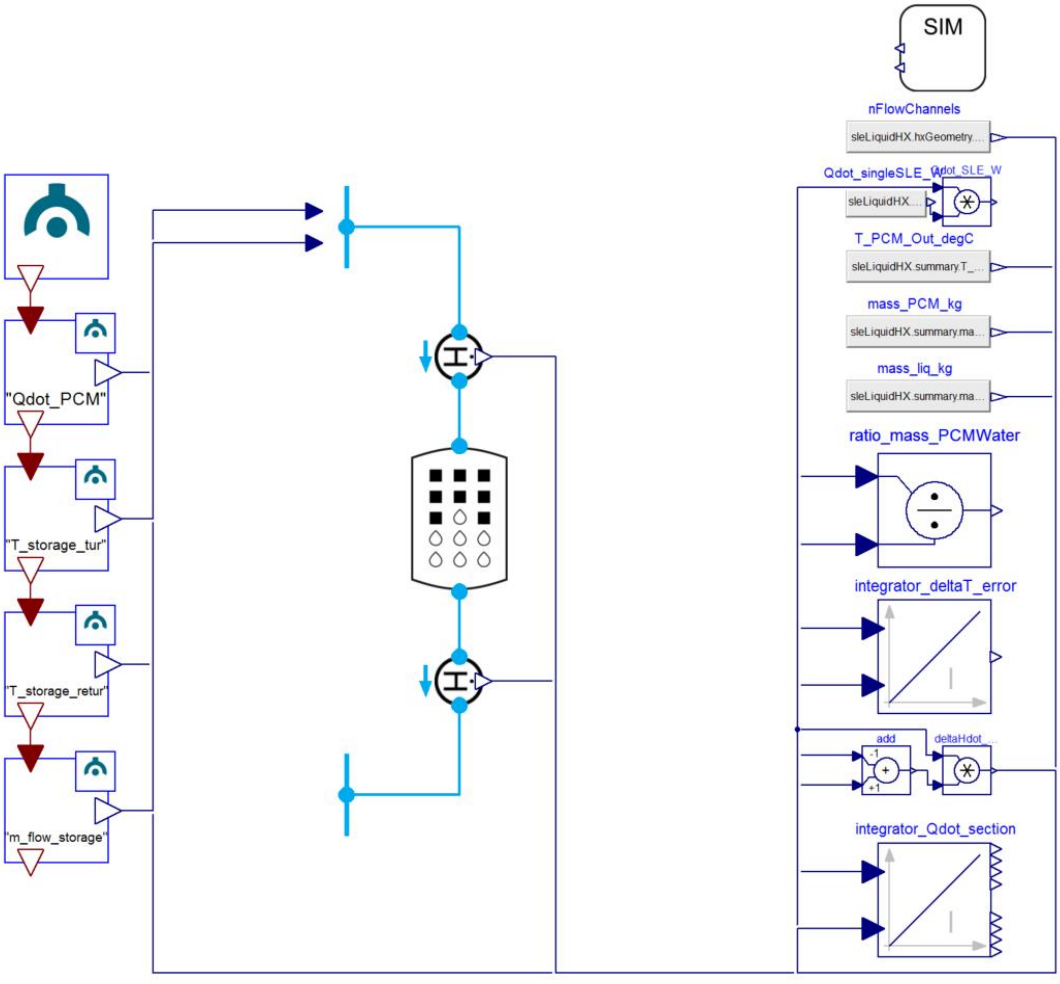

Figure 11 – Interface of the PCM heat exchanger model (Simulation environment: Dymola)

The setup consists basically of three main parts:

In the upper right corner is the SIM-block. It provides the required material data and properties of the liquid (water), the PCM (salt hydrate, type "S10", manufacturer PCM Products Ltd.) and the container's wall (high-density polyethylene, HDPE).

On the left hand side in figure 11 are the file reader blocks, which provides the measurement data for the simulation. More information about the utilized measurement data is given in chapter 4.

The measurement data is used as an input for the actual PCM heat exchanger block in the middle of figure 11. The HX block is estimating the heat transfer rate between a layer of PCM containers and the half of its surrounding flow channel on each container side. The corresponding system boundaries for the model are shown in figure 12.

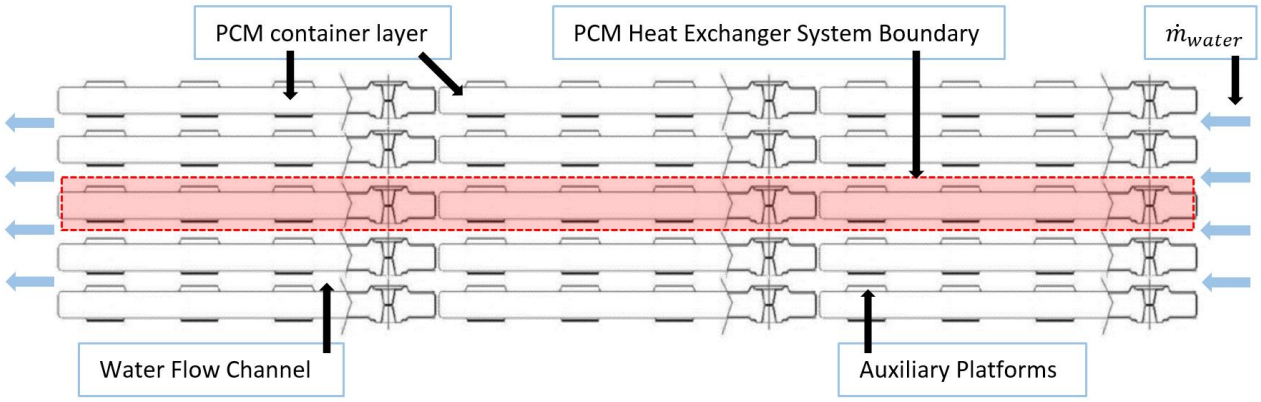

Figure 12 – Side view of the tank's internal scheme

Since the water is assumed to be equally distributed over the cross-sectional area, the heat transfer rate will be the same for each particular container layer. After the heat transfer rate for one layer ($\dot{Q}_{PCM,container\ layer}$) has been calculated, it will be multiplied with the total amount of flow channels to compute the tank's overall heat transfer rate ($\dot{Q}_{PCM}$). The disadvantage of this method is that the tank material itself (i.e. the mass of the steel wall) is not considered in the calculation. This simplification is discussed in detail in the validation chapter 4.

The remaining blocks on the right side in figure 11 are serving for performance analysis or debugging. The input parameters for the PCM storage model are listed in Table 1.

Table 1 – Parameter list for the PCM heat exchanger

Input Parameters – PCM Storage	
Discretization in Direction of the Flow Channel $\boldsymbol{n_{cells,flow\ channel}}$	Discretization in Direction of the PCM $n_{cells,PCM}$
Tank Height $\boldsymbol{h_{tank}}$ $[\boldsymbol{m}]$	Tank Width b_{tank} $[m]$
Tank Length $\boldsymbol{l_{tank}}$ $[\boldsymbol{m}]$	Number of Flow Channels $n_{flow\ channels}$
Container Wall Thickness $\boldsymbol{d_{wall}}$ $[\boldsymbol{m}]$	Flow Channel Height $h_{flow\ channel}$ $[m]$
Measured Inlet Water Temp. $\boldsymbol{T_{water,in}}$ $[°\boldsymbol{C}]$	Measured Mass Flow Rate $\dot{m}_{water}$ $[\frac{kg}{s}]$
Material Properties of the PCM	Material Properties of the Wall (HDPE)

In addition to the parameters presented in Table 1, the measured outlet water temperature $T_{water,out}$ and the measured cooling capacity $\dot{Q}_{PCM}$ will be utilized in the validation (see chapter 4).

The differentiation between the discretization in the direction of the flow channel and in the direction of the PCM is due to the internal structure of the PCM storage model, which will be discussed in chapter 3.3. Most of the required input parameters from table 1 are dependent on the dimension of both the PCM cold storage tank and the particular PCM containers, as illustrated in figure 13.

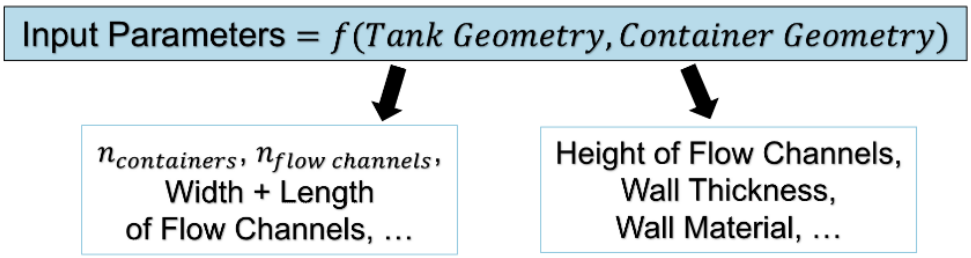

Figure 13 – Input parameters as a function of tank and container geometry

In addition, initial values are required as well (table 2). Initial values influence the quality of the model's calculations especially in the beginning of the simulation (see chapter 4.3.2).

Table 2 – Parameter list for initialization of the PCM heat exchanger

Initial Parameters – PCM Storage	
Freezing Progress in Direction of the Channel $\boldsymbol{x_{init,flow\ channel}}$	Freezing Progress in Direction of the PCM $x_{init,PCM}$
Water Temperature $\boldsymbol{T_{init,water}}$ $[°\boldsymbol{C}]$	Wall Temperature $T_{init,wall}$ $[°C]$
PCM Temperature $\boldsymbol{T_{init,PCM}}$ $[°\boldsymbol{C}]$	

The PCM cold storage tanks that are used in the University College of Bergen has been designed by the Swedish engineering consultancy company Sweco. Figure 14 shows the engineering drawing for a 57 m^3 PCM tank.

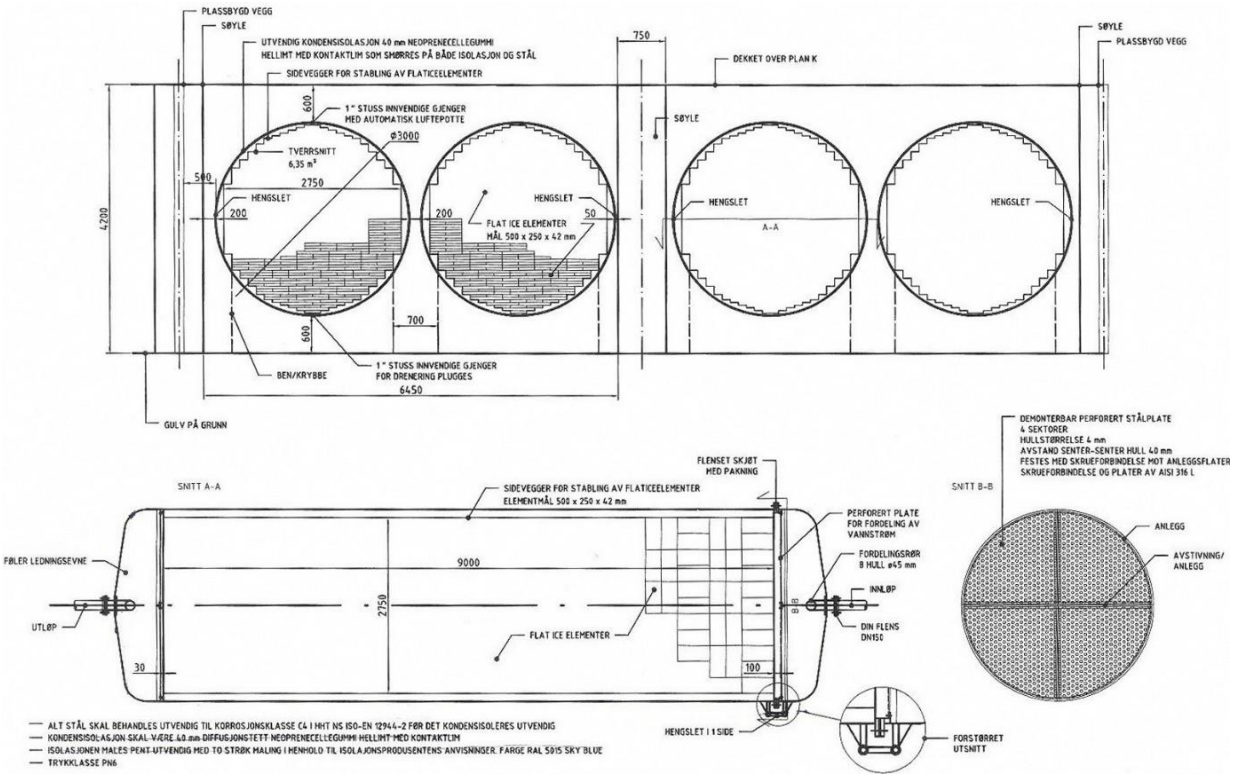

Figure 14 – Engineering drawing for the PCM cold storage tank (Sweco2014)

As mentioned in chapter 2.2, these tanks are filled with small containers that contain PCM. The containers are called FlatICE™ elements, provided by the British company PCM Products Ltd. The salt hydrate in these containers has a phase change temperature of 10 °C (PCM Products Ltd. 2011). Water flows through the tanks and through the small flow passage between the stacked PCM containers.

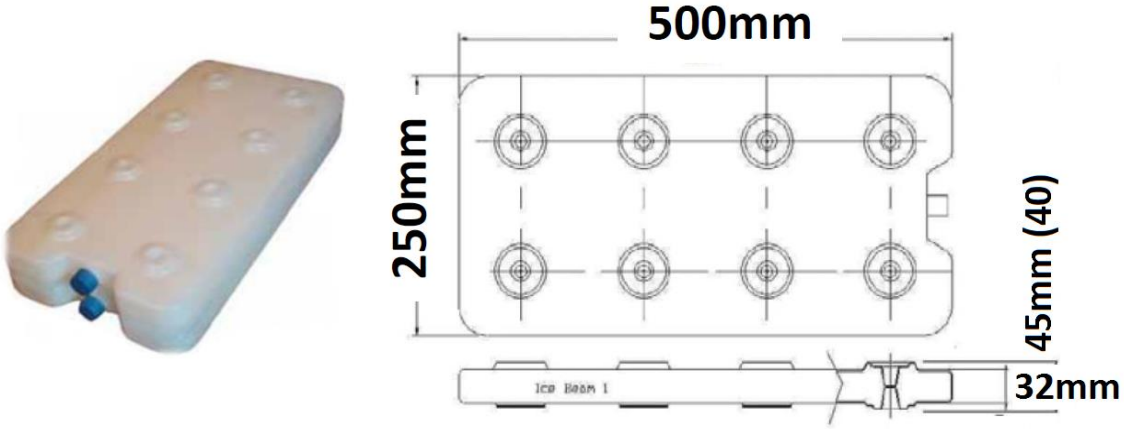

Figure 15 – Single FlatICE™ container (PCM Products Ltd. 2011)

Figure 15 shows the dimensions for a single PCM container. The nominal height is 45 mm. However, when several PCM containers are stacked on top of each other, squeezing occurs. This leads to a decreased height of the container. For that case, the manufacturer of the containers, PCM Products Ltd., suggests to assume a container height of 40 mm.

With all the provided geometric data from figure 14 and figure 15, the values for the flow channel dimensions and the input parameters in table 1 can be calculated.

The length of the water flow channel equals the length of the PCM tank.

$$l_{tank} = l_{flow\ channel} = 9\ m \tag{1}$$

The total cross-sectional area of the PCM tank is given in figure 14 with A = 6.35 m^2. Since the modelled PCM tank has a square shape (see derivation in chapter 3.1) and since the width of the flow channel equals the width of the overall tank (when the effect of the walls on the side is neglected), the width of the flow channel is

$$b_{tank} = b_{flow\ channel} = \sqrt{6.35\ m^2} = 2.52\ m \tag{2}$$

The height of the flow channel is the gap between two PCM containers. The gap is formed due to the small round auxiliary platforms of the containers, as shown in figure 15.

$$h_{flow\ channel} = 40\ mm - 32\ mm = 8\ mm \tag{3}$$

The total number of PCM containers that can be stacked within the PCM tank is the ratio between the tank height and the container height

$$n_{containers} = \frac{h_{tank}}{h_{container}} = \frac{2.52\ m}{0.04\ m} = 63 \tag{4}$$

Therefore the amount of flow channels is $n_{flow\ channels} = 63$ as well.

All these parameters will be used within the PCM heat exchanger model to estimate the performance of the storage. How the heat transfer is calculated will be discussed in detail in the following chapter.

3.3 Internal Structure

The PCM heat exchanger model consists basically of three different types of cells. Liquid cells are connected with the PCM cell over wall cells as shown in figure 16.

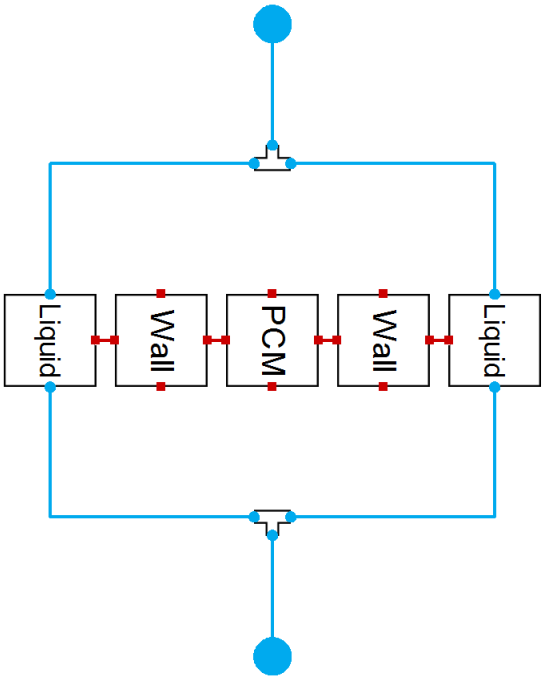

Figure 16 – Internal interface of the PCM heat exchanger model

Figure 16 shows the internal structure of the PCM heat exchanger model. This structure resembles the tank's internal scheme from figure 12. The discretization of the particular cells is possible along the water flow channel and in depth direction to the PCM. Therefore, $n_{cells,flow\ channel}$ and $n_{cells,PCM}$ are eligible parameter for the simulation. While $n_{cells,flow\ channel}$ affects the discretization of all three cell types, $n_{cells,PCM}$ is only discretizing the PCM cell into the direction of the heat transfer (which is perpendicular to the water flow direction).

The heat transfer rate in each cell is dependent on the type of heat transfer and will be discussed in detail in the following sections.

3.3.1 Liquid Cell

The energy balance equation for the liquid cell is

$$m_{water} * c_p * \frac{dT_{water}}{dt} = \dot{m}_{in} * h_{in} + \dot{m}_{out} * h_{out} + \dot{Q} \tag{5}$$

For the present case, three different options for the heat transfer type are possible: Conduction, natural convection or forced convection. Whether the dominating type of heat

transfer is conduction or convection, can be deduced from the Rayleigh number (Ra), a dimensionless number in fluid mechanics. It is calculated as

$$Ra = \frac{c_p * \rho * g * \beta * \Delta T * l^3}{\upsilon * \lambda} \tag{6}$$

With applying the gravitational acceleration g in m/s^2, the thermal expansion coefficient β in K^{-1}, the characteristic length l in m, the kinematic viscosity υ in m^2/s and the thermal conductivity λ in W/mK.

Computing the Rayleigh number for several possible boundary conditions for the present case lead always to a Rayleigh number of > 1700, which indicates that forced convection is the dominant heat transfer type for the liquid cell.

The heat transfer rate for forced convection is

$$\dot{Q}_{water} = \alpha_{water} * A * \left(T_{port} - T_{water}\right) * k_{temp\ dependence} \tag{7}$$

The heat transfer area A describes the area between water and wall. For example, in case of a single PCM container with a discretization of 1 into every dimension, the heat transfer area would be $0.5\ m * 0.25\ m = 0.125\ m^2$ (see figure 15).

The factor $k_{temp\ dependence}$ considers the change of the water's thermophysical properties as a result of a changing temperature between the water directly at the wall and in the middle of the flow channel (VDI Heat Atlas 2013):

$$k_{temp\ dependence} = \left(\frac{Pr}{Pr_{atWall}}\right)^{0.25} \tag{8}$$

Finally, to calculate the heat transfer coefficient α_{water} and to describe the forced convective heat transfer for the particular case of a PCM heat exchanger, several possible cases can be found in literature. The validation showed that the best simulation results are obtained when assuming the case "flow over a horizontal plane", followed by the case "flow in a flat gap between two heated walls". The equations and the simulation results for the case "flow in a flat gap between two heated walls" will be given in the appendix chapter A.7.

For the case "flow over a horizontal plane", the heat transfer coefficient becomes (VDI Heat Atlas 2013):

$$\alpha_{water} = \frac{k_{freeze\ time} * \lambda * Nu}{l_{flow\ channel}} \tag{9}$$

The freezing time factor $k_{freeze\ time}$ is considering the effect, that the time for freezing the PCM is greater than the time for melting the PCM. Further information and a calculation of this factor will be given in the section 3.3.3 of PCM heat transfer in the end of this chapter.

The Nusselt number can be calculated from

$$Nu = 0.664 * \sqrt{Re} * Pr^{\frac{1}{3}} \tag{10}$$

This equation is valid for laminar flows with $Re <$ (1^5). Chapter 4 will show a maximum water volume flow of up to 100 m^3/h, resulting in a Re of slightly higher than 1^5. However, tests with a Nusselt number for turbulent conditions resulted in only minor changes to the overall quality of the simulation results.

The corresponding Reynolds number is

$$Re = \frac{l_{flow\ channel} * v * \rho}{\eta} \tag{11}$$

With applying the dynamic viscosity η in $kg/(ms)$ and flow velocity v of

$$v = \frac{\dot{m}}{\rho * A_{flow\ channel}} \tag{12}$$

The calculation of the flow velocity might be inaccurate, since the small auxiliary platforms of the PCM containers are affecting the flow conditions within the rectangular flow channels. This effect was however neglected in the present study

Applying equations 7 – 12, the convective heat transfer in the liquid cell can be estimated.

3.3.2 Wall Cell

The energy balance equation for the wall cell is

$$m_{wall} * c_p * \frac{dT_{wall}}{dt} = \dot{Q}_{wall,portN} + \dot{Q}_{wall,portS} + \dot{Q}_{wall,portW} + \dot{Q}_{wall,portE} \tag{13}$$

While the liquid cell only possesses one single heat port that connects the liquid cell with the adjacent wall cell, the wall cell itself possesses four heat ports. Two of them are connected to the liquid cell (port "S") and the PCM cell (port "N"). The remaining two ports on the side

of the wall cell are connected to the previous (port "W") and next wall cell (port "E"), in case of a discretization of $n_{cells,flow\ channel} > 1$.

For this case the heat transfer type is clearly just heat conduction. The respective heat transfer rates are calculated for each heat port separately:

$$\dot{Q}_{wall,portX} = \frac{T_{portX} - T_{wall}}{R_X} \tag{14}$$

With R_X as the heat resistance in Km/W, which is dependent on the direction of the heat transfer. The heat resistance in the direction of the heat transfer is

$$R_{NS} = \frac{d_{wall}/2}{\lambda_{HDPE} * A_{NS}} \tag{15}$$

And in the direction perpendicular to the heat transfer the heat resistance is

$$R_{WE} = \frac{l_{WE}/2}{\lambda_{HDPE} * A_{WE}} \tag{16}$$

The "NS" and "WE" subscripts are identifying the particular cross-section areas for calculating the heat resistance in the direction of the tank's length ("WE") and in the direction of the tank's width ("NS"). Thus, R_{NS} is the heat resistance for the heat transfer between water and PCM, and R_{WE} is the heat resistance for the heat transfer between the particular wall cells.

3.3.3 PCM Cell

The balance equation for the PCM cell is

$$m_{PCM} * \frac{dh_{PCM}}{dt} = \dot{Q}_{PCM,portN} + \dot{Q}_{PCM,portS} + \dot{Q}_{PCM,portW} + \dot{Q}_{PCM,portE} \tag{17}$$

The main difference to the balance equations of the liquid and wall cell is the use of the derivation of the enthalpy instead of the derivation of the temperature, because the proper calculation of the thermal capacity c_p in the area of the phase change is nontrivial.

The determination of the heat transfer type for the PCM cell is quite challenging. In the case of a completely frozen PCM the heat transfer will be just heat conduction. But as soon as the PCM starts to melt, the heat transfer type will start to change. On the one hand the thermal conductivity λ will alter with the change of the phase and the liquid mass fraction x. On the other hand, as soon as molten PCM is formed, it will start to move within the PCM container,

leading to a heat transfer that resembles natural convection. The same applies for complete liquid PCM. The part of the PCM that is close to the wall will change its temperature and thus its properties. That way a changed buoyancy can lead to small mass flows within the container, affecting the heat transfer type. Finally, the most challenging case is the beginning of freezing. The emerging and increasing layer of frozen PCM directly at the wall might act as some sort of an isolator for the remaining liquid PCM, leading to a higher freezing time than melting time for PCM storages (see freezing/melting profiles in chapter 4.1).

Libeer (2016) proposes the following explanation for the huge difference in the melting and freezing time: The convective heat transfer rate is highly dependent on the buoyancy force that is dominant during the melting of pure PCM. Fluctuating liquid water within the PCM cell is increasing the heat transfer rate. That way, the time to melt the PCM decreases drastically in comparison to the freezing process.

Sun (2015) explains the time difference of the phase changes with the temperature difference within the PCM container as well. The temperature difference enhances the natural convection within the cell, since liquid PCM has a lower density and viscosity than the solid PCM. With progressing PCM melting, liquid PCM continues to move to the top of the container while the solid PCM descends to the bottom, thus enhancing the melting process and reducing the melting time. Therefore, the heat transfer rate for horizontally aligned PCM containers is higher on the lower side of the PCM containers than on the upper side.

In recent years the effort in researching the phenomena of heat transfer that is related to PCM has greatly increased. Figure 17 shows the number of published papers related to the topic. The number of published papers is raising each year. This shows on the one hand the increased attention towards the topic of PCM thermal storage. On the other hand it shows the need for further research on the topic of phase change related heat transfer. General understanding of the PCM heat transfer is required as well as more detailed equations to describe the heat transfer for a PCM with appropriate quality.

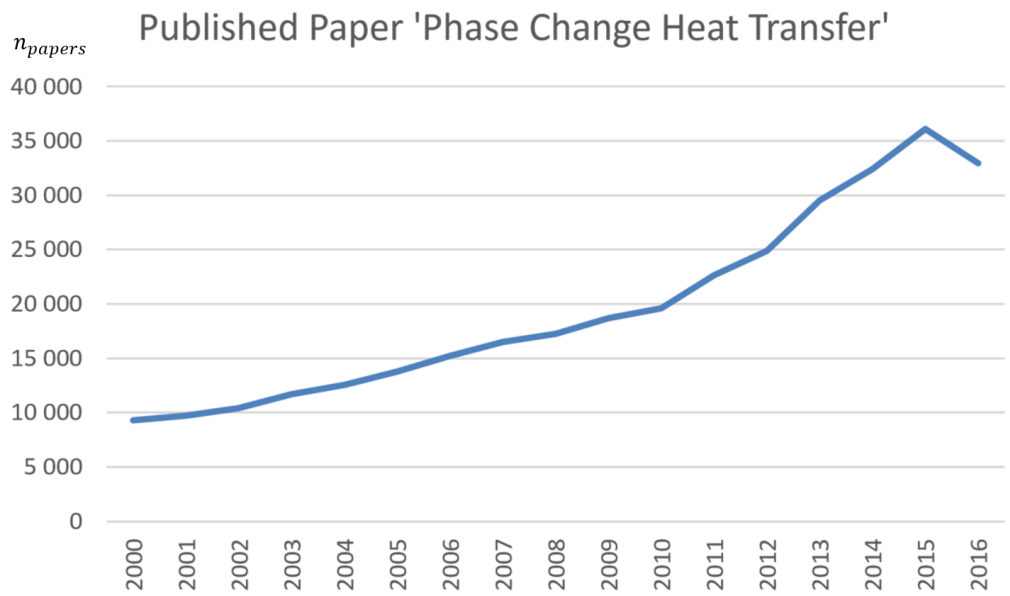

Figure 17 – Numbers of published papers related to the topic of "phase change heat transfer" (ScienceDirect.com, July 2016)

At present, for the model utilized in this project report, it is assumed that the heat transfer type is mere heat conduction nevertheless. Thus, the applied equations for PCM cell are analogous to the equations applied to the wall cell (equations 14 – 16).

$$\dot{Q}_{PCM,portX} = \frac{T_{portX} - T_{wall}}{R_{NS}} \tag{18}$$

$$R_{NS} = \frac{d_{wall}}{2 * \lambda_{PCM} * A_{NS}} \tag{19}$$

$$R_{WE} = \frac{l_{WE}}{2 * \lambda_{PCM} * A_{WE}} \tag{20}$$

To consider at least the general difference between melting and freezing time, a factor $k_{freeze\ time}$ is introduced in the heat transfer equations for the liquid cell (see equation 9). This factor was implemented into the liquid cell instead of the PCM cell, since it is easier to affect the model's performance with changes of the heat transfer coefficient of the liquid side than with changes of the heat transfer resistance of the PCM cell. Therefore it was decided that the freezing progress of the PCM cell is directly affecting the heat transfer coefficient of the water α_{liq}, utilizing the factor $k_{freeze\ time}$:

$$\alpha_{liq} = f(k_{freeze\ time}) \tag{21}$$

The factor $k_{freeze\ time}$ is a function of the liquid mass fraction of the PCM. To compute $k_{freeze\ time}$, a polynomial regression function is used:

$$k_{freeze\ time} = f(x_{PCM}) = ax^3 + bx^2 + cx + d \quad (22)$$

The parameters for the regression function are adjusted such that the heat transfer coefficient becomes smaller when the molten PCM starts to freeze. Figure 18 shows the model's setup for calculating $k_{freeze\ time}$.

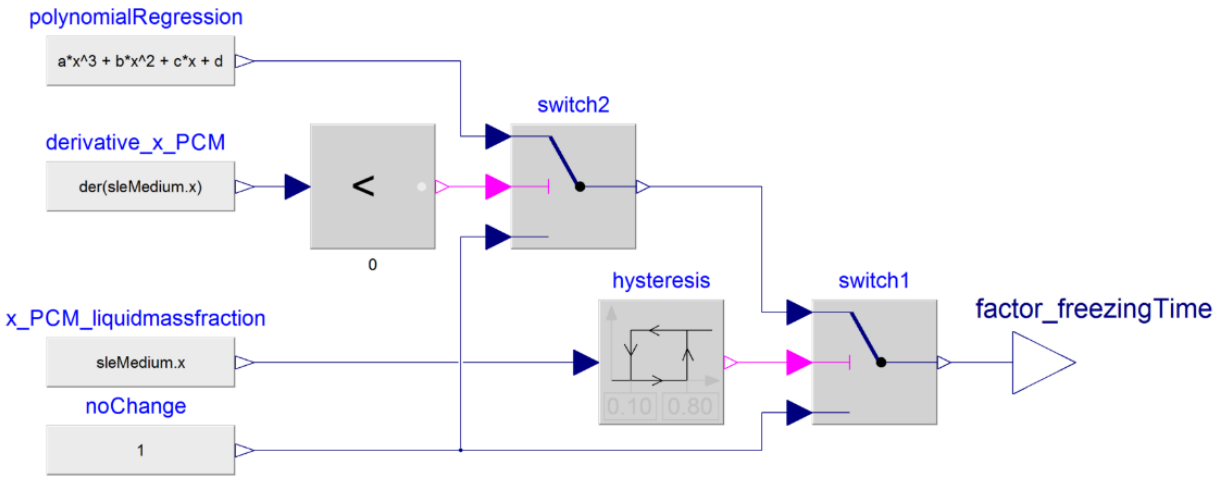

Figure 18 – Calculation of the freezing time factor $k_{freeze\ time}$

Most of the time, $k_{freeze\ time}$ equals one. It will decrease to a lower value (< 1) and thus start to slow down the heat transfer rate as soon as $\frac{dx}{dt}$ becomes negative, which implies the start of freezing. As discussed before, the freezing process of the PCM is increasingly covering the wall with frozen PCM, leading to a delayed heat transfer in comparison to the melting processes. However, to keep $k_{freeze\ time}$ from delaying the heat transfer every single time a partial or only transient freezing process occurs, a hysteresis is added to ensure the factor $k_{freeze\ time}$ is just taking action for cases when it is actually required.

All the equations required for describing the heat transfer of the PCM heat exchanger have now been introduced. Therefore, the introduction of the model's internal structure is completed and the following chapter will discuss the validation results and performance evaluation.

4 Validation

In this chapter the simulation results will be compared with measurement data to assess the accuracy and quality of the PCM storage model. For that purpose the British PCM manufacturer PCM Products Ltd. and the Swedish engineer company Sweco provided several sets of freezing/melting profiles and measurement data.

Three different data sets were available. Each of these will be used for validation in the following chapters. The complexity of the validation will increase with each chapter.

In chapter 4.1, the melting and freezing profiles will be used to verify the model's estimations for the freezing and melting time, with a constant mass flow and a constant inlet temperature.

Chapter 4.2 utilizes measurement data from the PCM storage at the University College in Bergen, thus the inlet temperature changes over time and the model's dynamic response can be evaluated. However, only limited phase change processes occur during the recorded time period and the focus of the validation lies on the correct calculation of the sensible heat transfer.

Finally, in chapter 4.3 measurement data with highly dynamic operation modes is utilized. The model needs to consider the changing inlet temperature and changing inlet mass flow. Furthermore, actual charging and discharging cycles with complete freezing or melting cycles need to be predicted by the model. The chapter concludes with an evaluation of the general measured PCM tank performance.

4.1 Freezing and Melting Profiles 2011

Freezing and melting profiles serve to describe the general behaviour of a PCM in regard to its performance during phase change processes. Every PCM features individual characteristic freezing and melting profiles.

The profiles used in this chapter are provided by the PCM manufacturer PCM Products Ltd. Table 3 compares the measured values taken from the PCM Products Ltd. profiles with the predicted values from the model. Figures 19 and 20 compare the trajectory of the measured and predicted freezing and melting profiles, respectively, as a function of the temperature difference.

Table 3 – Measured and predicted freezing and melting time

Temperature Difference ΔT	Measurement $t_{freezing}$	Model $t_{freezing}$	Measurement $t_{melting}$	Model $t_{melting}$
2	800	885	390	400
3	625	590	310	270
4	500	440	250	200
5	400	355	200	160
6	320	295	165	135
7	260	255	135	115
8	220	220	115	100
9	190	195	100	90
10	180	175	90	82

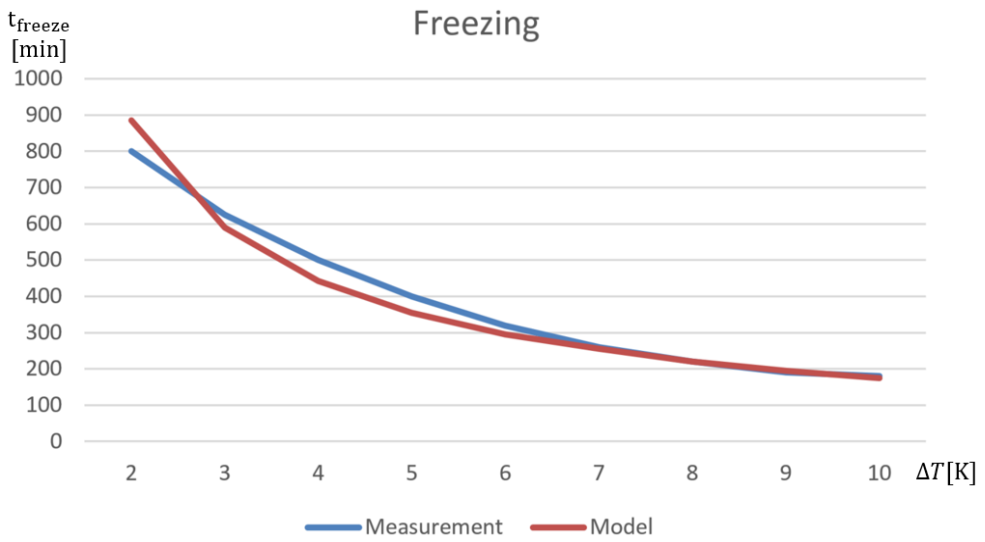

Figure 19 – Measured and predicted freezing times for varying temperature differences in min

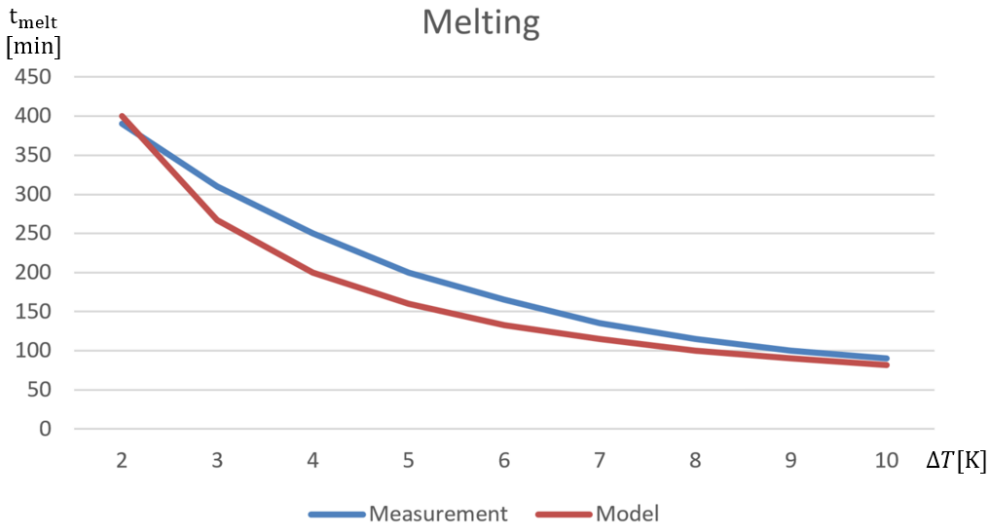

Figure 20 – Measured and predicted melting times for varying temperature differences in min

The temperature difference is the difference in temperature between the supplied water and the PCM, which is kept close to the freezing/melting temperature point. Thus, the freezing and melting time decreases with increasing temperature difference. As already discussed in chapter 3.3, the melting time is only half of the freezing time.

Based on figures 19 and 20, the model is capable of estimating the correct trajectory for the freezing and melting time. Unfortunately, no information was available about the mass flow that was applied when the measured profiles were recorded. However, as shown in chapter 3.3, the heat transfer coefficient is a function of the Reynolds number and thus of the mass flow rate. The heat transfer rate is different for every mass flow. The mass flow rate for the model was set to 10 m^3/h, a value taken from the measurement sets of the following chapters.

Therefore the freezing and melting profiles can be just utilized for a very preliminary validation to reproduce the general trajectory for the freezing time and melting time. Furthermore, the freezing and melting profiles were used to adjust the parameters of the regression function (equation 22) to calculate the freezing factor $k_{freeze\,time}$ (section 3.3). Without the freezing factor the values for the freezing and melting time would be almost equal.

4.2 Measurement at University College of Bergen in 2015

The following measurement data set of the PCM cold storage performance was collected by Sweco from 01.06.2015 until 26.07.2015 at the University College in Bergen, during normal operation of the building and the energy system. The PCM cold storage was little used during the investigated period. Because of summer vacations, few people were present in the building, and the weather was rather cold, leading to a low cooling demand. Therefore the cooling capacity from the heat pump together with the adiabatic cooling system were sufficient to supply the building's cooling demand.

Nevertheless, the data set can be used to validate the PCM storage model in the region of sensible heat transfer with $T_{PCM} < 10\ °C$ and a liquid mass fraction of x = 0. The particular measurement data set that was utilized for the validation of the model consists of: supply and return temperature $T_{water,in}$ and $T_{water,out}$, the mass flow rate $\dot{m}_{water}$ into the PCM tanks, and the cooling capacity $\dot{Q}_{PCM}$ of the PCM storage.

The values for the inlet temperature and the mass flow rate are used as input parameters for the model. The measured outlet temperature and cooling capacity serve for the comparison to the predicted outlet temperature and the predicted cooling capacity by the model.

4.2.1 Measurement 07.06.2015 – 09.06.2015

The first measurement excerpt used for the validation is a two days recording with just sensible heat transfer, no phase change and a constant mass flow rate.

Figures 21 – 23 illustrate the general operation mode of the PCM storage during the measured two days. The inlet temperature of the water was only changing by 2 K. For the first twelve hours the inlet and outlet temperature are the same, implying a system in a steady state. Thus, the heat transfer rate is zero as well (figure 23). In the subsequent hours the inlet temperature starts to fluctuate. The model is capable of estimating the correct outlet temperature from the PCM tank. However, each time a local peak occurs in the outlet temperature, the model is struggling with calculating the correct temperature. Figure 23 shows at 08.06. 13:00 that the modelled PCM storage is not capable to provide an appropriate heat flow rate to keep the outlet temperature above the inlet temperature. A reason might be that the steel tank mass was not considered (see chapter 3.2). With an additional thermal mass that is capable of saving thermal energy during the steady state operation mode before, the predicted outlet temperate could have kept closer to the initial temperature of 8 °C and thus closer to the measured outlet temperature. However, quite satisfying validation results are obtained with progressing measurement data. After 08.06. 19:00 both the simulated and measured outlet temperature are very close. The same applies for the simulated and measured heat transfer rate in figure 23.

In the next step, to increase the complexity of the inputs for the model, the following measurement data set will provide a changing mass flow rate.

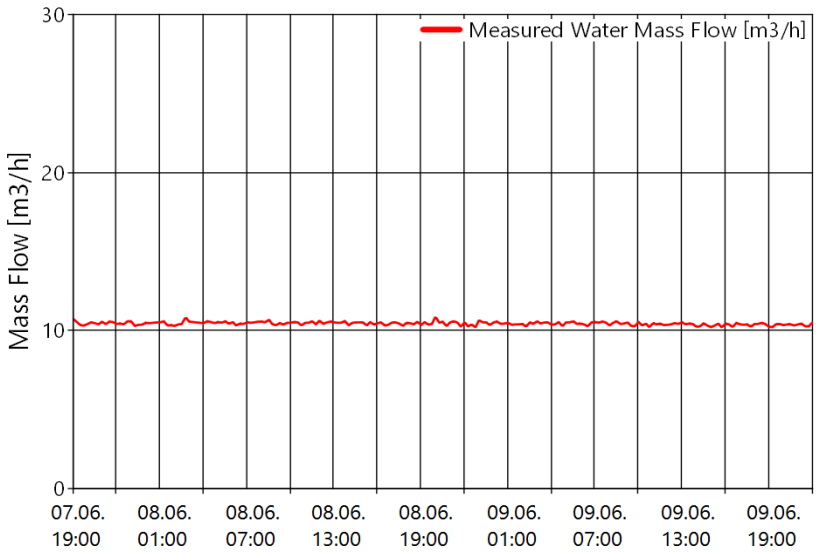

Figure 21 – Measurement 07.-09.06.2015, water mass flow rate in m^3/h

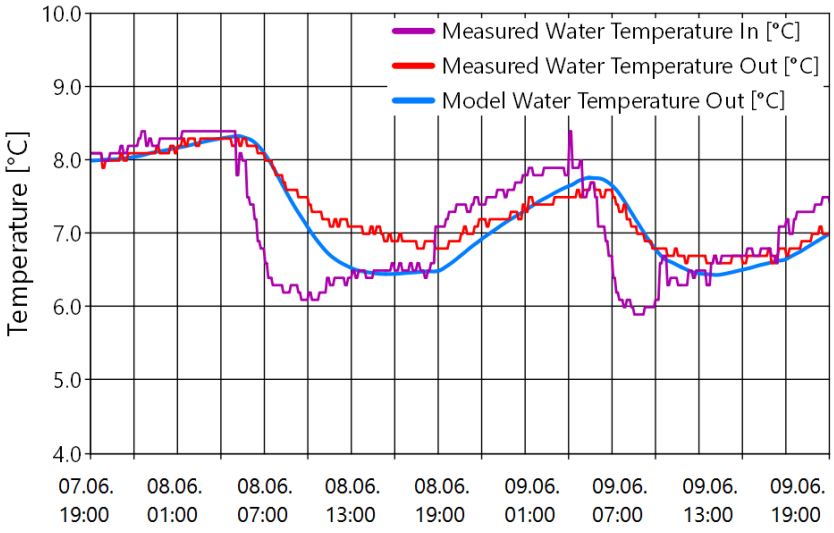

Figure 22 – Measurement 07.-09.06.2015, water inlet and outlet temperature in °C

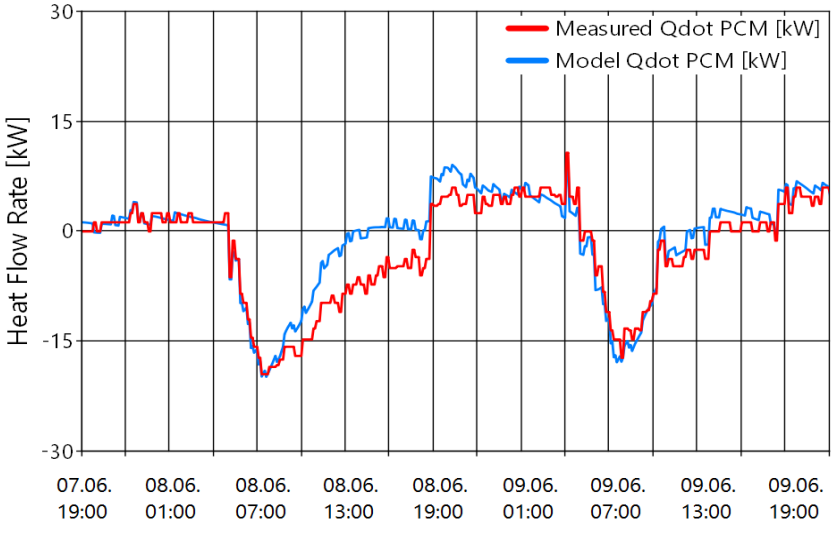

Figure 23 – Measurement 07.-09.06.2015, heat transfer rate of the PCM in kW

4.2.2 Measurement 21.06.2015 – 23.06.2015

Figures 24 – 26 present measured and simulated data from another period in 2015. The main difference in this data set in comparison to the measurement from June 7th is the varying water mass flow rate and a short time period with partial melting. The first hours consist of a steady state operation mode, leading to a heat flow rate of approximately zero, as shown in figure 26. After 24 hours, at 22.06. 12:00, the mass flow decreases to zero for roughly six hours (figure 24). When the water mass flow increases again, the inlet water temperature has increased from 9 to 17 °C, causing a partial melting process of the formerly frozen PCM (figure 25). At 22.06. 23:00 the inlet temperature is decreased to 9 °C again, leading to a decreasing outlet water temperature that is slowly converging towards T_{in}.

The model predicts the outlet water temperature with a proper tendency, as it can be seen in figure 25. During the period when no mass flow occurs (starting at 22.06. 12:00) the predicted outlet temperature remains the same, while the measured outlet temperature increases. This results from the increasing inlet temperature, since figure 26 shows that there is no heat transfer from the PCM during this time period. Despite this minor inaccuracy of the model during that special operation mode, the outlet temperature is predicted correctly again when the mass flow is applied at 22.06. 17:00.

After the mass flow increases again the inlet temperature increases to 17 °C. The model calculates a slightly lower outlet peak temperature than the measured one. However, the simulated heat transfer rate is exactly the same as the measured one during that period. An explanation might be that the fluctuating mass flow has caused inaccuracies for the temperature sensor, since a manual calculation of the heat transfer rate for this particular point leads to the same outlet temperature the one given by the model.

After the inlet temperature has decreased to 9 °C again at and after the PCM starts to completely freeze again at 23.06. 23:00, the model predicts an outlet temperature close to the melting temperature of 10 °C, which is approximately 0.5 °C higher than the measured outlet temperature. This difference might arise from the improper calculation of the heat transfer during the dynamic phase change. Partial melting and freezing processes impact the heat transfer rate, since the local boundary conditions directly at the PCM container wall are changed for every particular liquid mass fraction x. As discussed in chapter 3.3, adequate equations to predict this specific behaviour in a more detailed way are currently lacking.

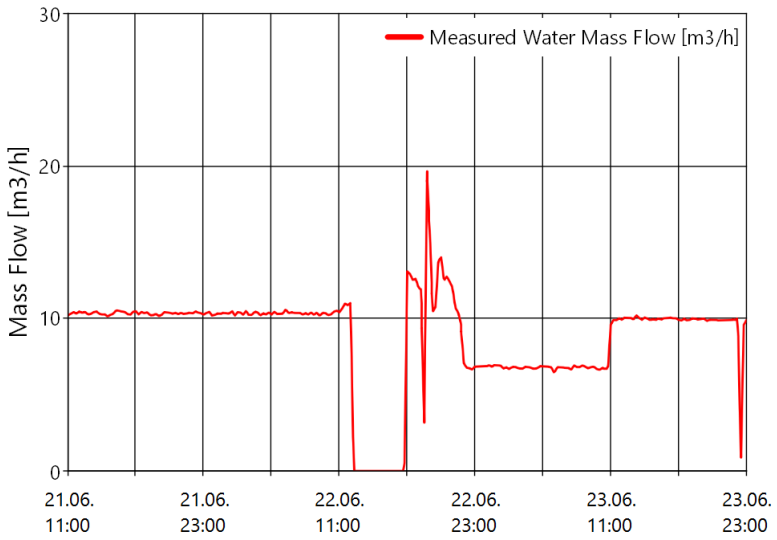

Figure 24 – Measurement 21.-23.06.2015, water mass flow rate in m^3/h

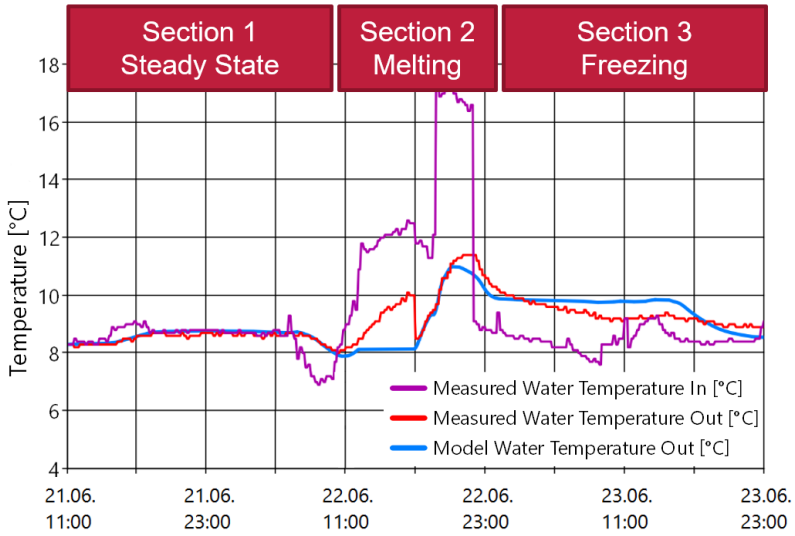

Figure 25 – Measurement 21.-23.06.2015, water inlet and outlet temperature in ℃

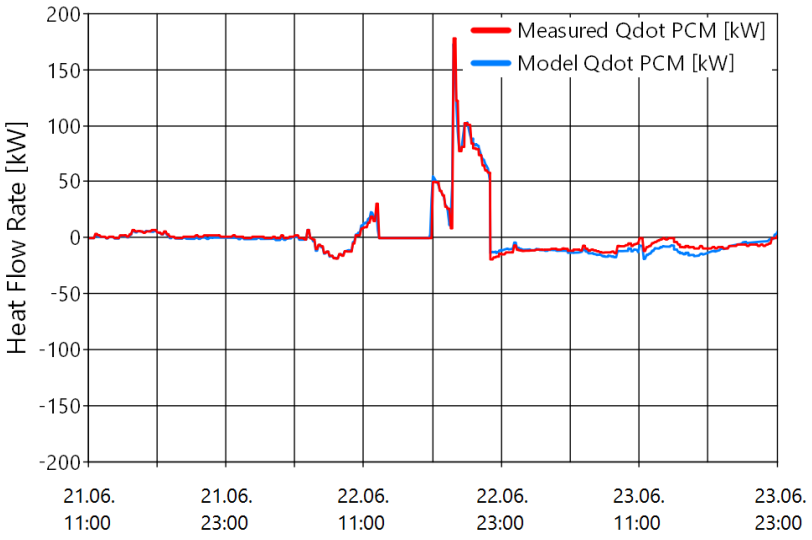

Figure 26 – Measurement 21.-23.06.2015, heat transfer rate of the PCM in kW

Nevertheless the results of the model's calculations are satisfactory. Figure 27 shows the results of the live simulation after the end of the measurement period at 23.06. 23:00. The yellow blocks on the right hand side in figure 27 show the measured and modelled integrated heat transfer rates and thus the amount of energy the PCM has absorbed and released during the investigated time period.

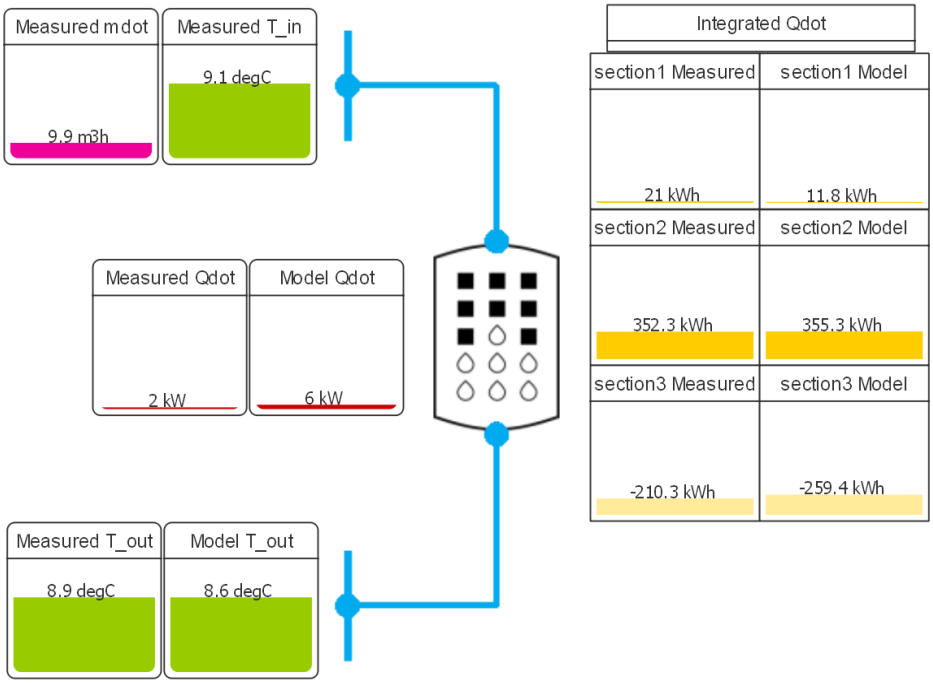

Figure 27 – Simulation end results for measurement 21.06.-23.06.2015

Section 1 ends at 22.06. 11:00 and covers the time period when outlet and inlet temperature are roughly the same. The integrated heat transfer for that section (first row of yellow blocks in figure 27) correctly implies that almost no energy was transferred during that steady state operation mode.

Section 2 starts when the mass flow increases again and ends when the inlet temperature decreases to 9 $°C$ at 22.06. 23:00. It represents the melting section and the model successfully estimates the correct amount of transferred energy for that period (second row of yellow blocks in figure 27). The remaining part of the simulation is covered by section 3, displaying the freezing part. As mentioned in the discussion above, the modelled PCM is releasing too much energy during this section (20 % more than the measurement) leading to an increase in the predicted outlet temperature. The graphs for the particular integrated heat transfer rates as a function of the time are given in the appendix. These graphs will be presented in the appendix for each of the subsequent chapters as well.

In general the validation of the model after applying the measurement data sets from 2015 is quite satisfactory. With the measurement of June 7th the estimated water outlet temperature was predicted too close to the measured water inlet temperature. On the contrary, with the measurement of June 21st the estimated water outlet temperature was too close to the PCM storage temperature. Nevertheless the overall deviation of the simulated outlet temperature from the measured outlet temperature was quite low. Figure 54 in the appendix A.3 illustrates that the deviation between estimated and measured outlet temperature is generally less than 0.5 K for the whole measurement data of 2015.

The chapter illustrated some inconsistencies between the simulation and the measurement. With these deviations in mind, the following measurement data set will focus on evaluating the PCM storage behaviour in connection to complete charging and discharging cycles.

4.3 Measurement at University College of Bergen in 2016

The measurements presented in this section were conducted by Sweco from 30.05.2016 until 05.06.2016. For several days in the recorded time period the PCM storage setup was run in a test mode. Instead of supplying all four PCM tanks with water, only one single tank was operated while the others were bypassed. Since the measurement data of 2015 illustrated that the PCM storage tanks were barely in use, an operation mode with only a quarter of the original amount of PCM mass is supposed to provide new information about the freezing and melting processes with preferably complete freezing/melting of the PCM tank. The overall system performance during the charging and discharging cycles and the actual status of the particular tanks could hence be better evaluated.

4.3.1 Measurement 30.05. – 01.06.2016 (4 sections)

Measured and simulated data for the mass flow rate, inlet and outlet temperatures and heat flow rate from 30.05. – 01.06.2016 is shown in figures 28, 29 and 30, respectively. The test mode with only PCM tank #1 in operation started from May 30th 11:30 and lasts until June 1st 5:30. During that time the tank is operated in a highly dynamic operation mode and performs four charging/discharging processes. This is the reason for calling this chapter "4 sections". In the subsequent chapter the same measurement data will be investigated, but with only three charging/discharging sections to stress the importance of the initialization of the model.

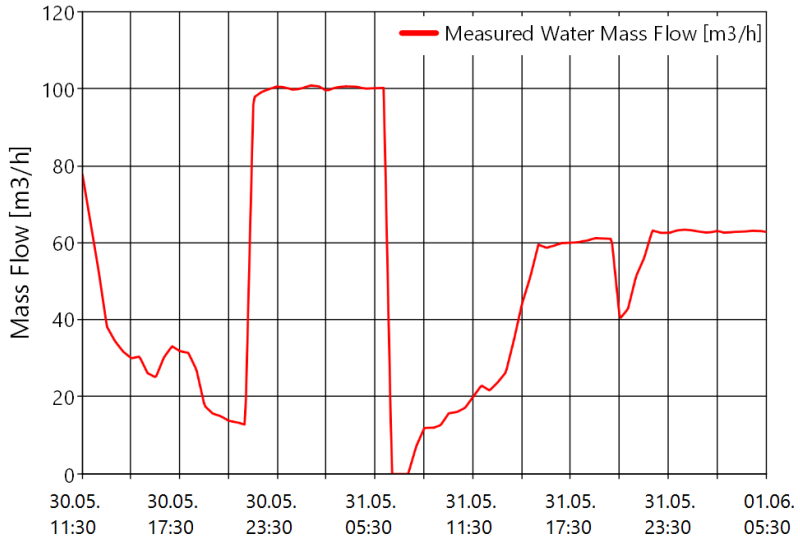

Figure 28 – Measurement 30.05.-01.06.2016 (4 sections), water mass flow rate in m^3/h

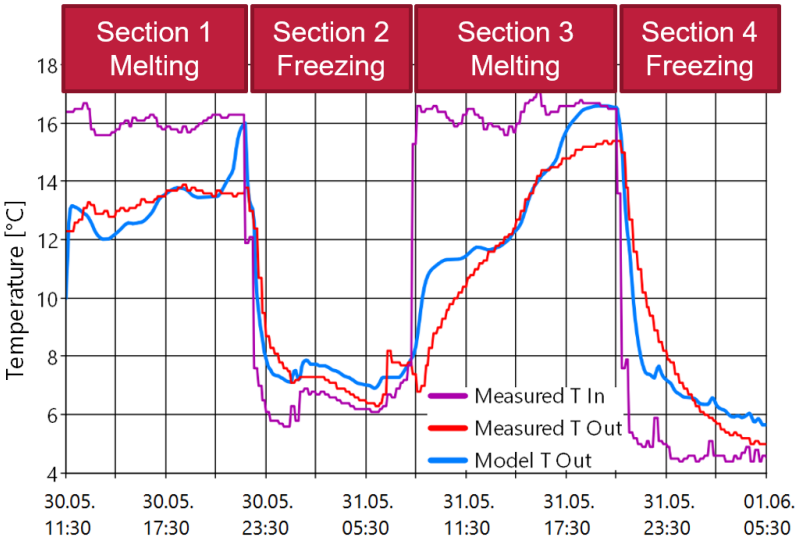

Figure 29 – Measurement 30.05.-01.06.2016 (4 sections), water inlet and outlet temperature in °C

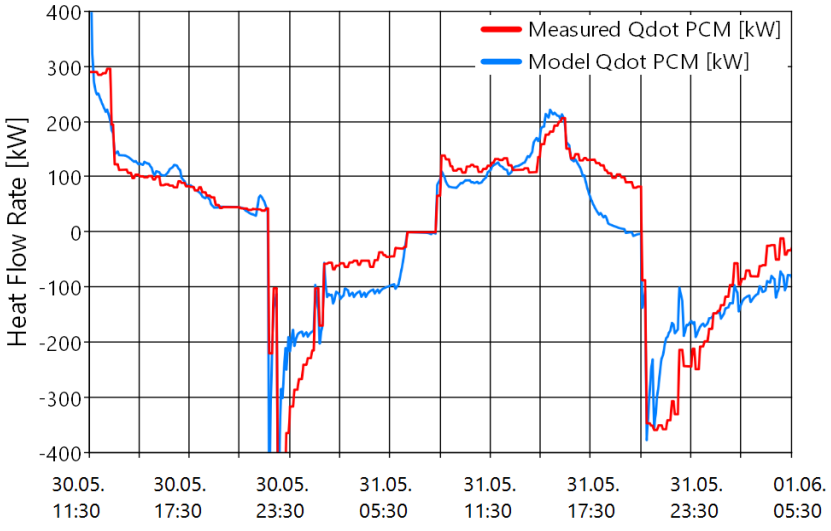

Figure 30 – Measurement 30.05.-01.06.2016 (4 sections), heat transfer rate of the PCM in kW

Apart from a very short period in the middle of the measurement period, the mass flow was constantly higher than zero (figure 28). The inlet water temperature was varying between 16 $°C$ for the melting sections and 5 – 6 $°C$ for the freezing sections (figure 29). The model is capable of reproducing the general trajectory of the measured outlet temperature.

The biggest deviations of the model's estimation, especially in regard to the predicted heat transfer rate, occurs in the melting sections (1 and 3 in figure 29). Both in section 1 and in section 3 the predicted outlet temperature is missing the correct value for the outlet temperature during the very beginning and during the very end of the respective section. A reason might be that in chapter 3.3 only a factor for modifying the freezing time ($k_{freeze\ time}$) has been implemented to consider the effect of the freezing process on the ordinary heat transfer coefficient. However, figures 29 and 30 illustrate that the melting progress appears to have a larger impact on the heat transfer as expected. The ordinary heat transfer coefficient seems to be influenced by the melting process, but in a slightly moderated way than by the freezing process. Thus, a factor for the melting behaviour $k_{melting}$ is currently lacking and needs to be included in the model in the future.

As for the freezing in section 2 and section 4, the trajectory of the predicted outlet temperature resembles the one of the measured outlet temperature. Although the progress seems to be different for both trajectories, both are roughly converging towards the same temperature at the end of the section. The same observation is valid for the heat transfer rate, which has a different slope for the predicted and the measured value as well. The predicted heat transfer during the freezing process seems to increase too much during the very beginning of the section and remains on a slightly lower level than the measured heat transfer which seems to have a more consistent trajectory in general.

This chapter shows furthermore, that a general understanding and a thorough interpretation of the measured values is essential for improving the quality of the model. The measurement illustrates a tank behaviour that cannot be completely specified by appropriate equations yet. Figures 28 shows a varying mass flow rate of approximately 20 – 60 m^3/h for both melting sections, with a decreasing mass flow rate in section 1 and an increasing mass flow rate in section 3. However, the corresponding heat transfer rates for these sections (figure 30) remain on slightly the same level (50 – 100 kW for section 1 and 120 kW for section 2, with a transient peak of 200 kW). In comparison, the heat transfer

rates during the freezing sections 2 and 4 are altering more, between a value of roughly 0 – 400 kW, despite of a constant mass flow rate in section 2 and section 4 (100 m^3/h and 60 m^3/h, respectively). The trajectory of the heat transfer rates are very similar for both freezing sections, although the mass flow rate is differing by a factor of almost 2. Also, the measured outlet temperature seems to converge faster towards the value of the inlet temperature during the freezing sections than in the melting sections (figure 29). It appears the heat transfer rate during the freezing process in the tank is less dependent on the mass flow rate as supposed in chapter 3.3.1. The heat flow rate during melting processes seems to be steadier than the more fluctuating heat transfer rate in the freezing sections. Chapter 3.3.3 discussed several explanations for this differing behaviour of the PCM tank for freezing and melting processes.

Nevertheless, the validation of the model during the freezing sections is quite satisfying. Despite the slightly inaccurate trend of the trajectory of the heat transfer rate in section 2 and 4, the integrated values for the heat transfer rate in these sections are very similar, as shown by the model results at the end of the simulation in figure 31.

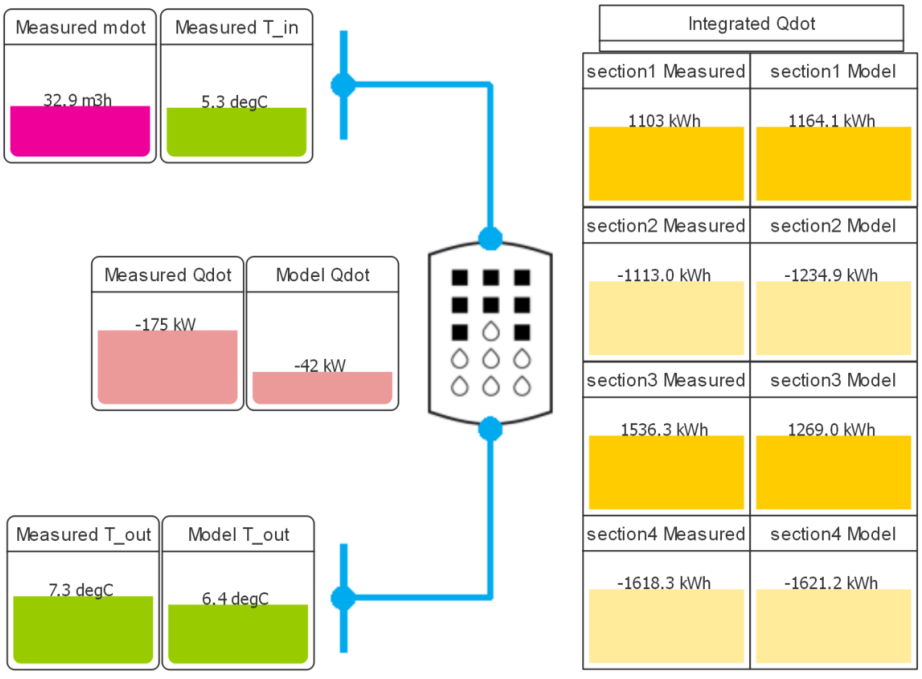

Figure 31 – Simulation end results for measurement 30.05.-01.06.2016 (4 sections)

In figure 31, the integrated values of the heat transfer for the freezing sections (section 2 and 4) are quite close, implying that the implementation of the factor for the freezing time $k_{freeze\ time}$ in chapter 3.3 was successful. However, figure 29 illustrated that the trajectory

of the predicted outlet temperature can be still improved. Thus, more research on defining the correct parameters of the regression function in equation 22 needs to be performed or an even more detailed estimation for the freezing behaviour needs to be implemented.

Figure 31 illustrates that especially in section 3 the values for the integrated heat transfer rate are deviating for the model's prediction and the measurement. As explained above, further research on the detailed melting behaviour is required to model the heat transfer in a more precise way.

Finally it shall be mentioned that the overall tank performance appears to be in a proper condition. The melting (discharging) sections are starting at 30.05. 11:30 and at 31.05. 08:30, respectively. They last for roughly 12 hours over the whole daytime until the night. The freezing (charging) sections start at 30.05. 21:00 and at 31.05. 20:00, respectively. They last for 12 hours during the night-time until the next morning. Therefore, the general operation of the PCM tank seems to fit the initial statements about the PCM storage performance that were discussed in chapter 2.2. Figure 31 tells that, as for the measured data, the amount of energy that was absorbed during section 1 (1103 kWh) equals roughly the amount of energy that is released again in section 2 (1113 kWh). The same applies for the subsequent sections, with absorbing about the same energy in section 3 (1536 kWh) that will be released again in section 4 (1618 kWh).

However, the initial design guides and preliminary calculations assumed a maximum cooling capacity of 2800 kWh per single PCM tank (see chapter 2). Although figure 29 illustrated that the measured outlet temperature has already begun to converge towards the inlet temperature in the end of section 2 and 4, and although the heat transfer rate in these freezing sections is converging to zero despite of rather high amounts of mass flow rates, it appears that nevertheless only 50 % of the available capacity of the PCM tank has been used. This result can be confirmed by the model, as shown in figure 32, illustrating the model's prediction of the liquid mass fraction for a discretization in the direction towards the flow channel of $n_{cells,flow\ channel}$ = 3.

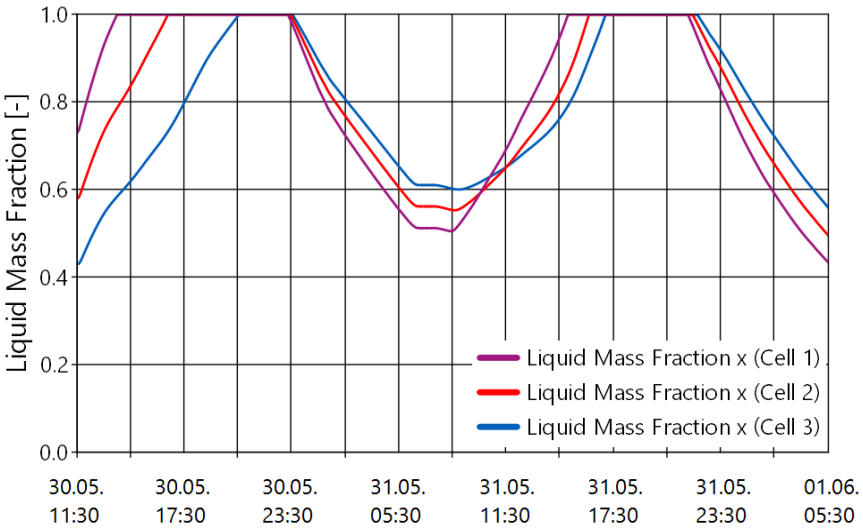

Figure 32 – Measurement 30.05.-01.06.2016 (4 sections), model's prediction of the liquid mass fraction with discretization of n = 3 (cell 1 at the front and cell 3 at the end of the tank)

The model predicts that the PCM storage is only partially melting, until a liquid mass fraction of x = 0.5 – 0.6, just as it was reasoned by comparing the integrated heat transfer rates above. Therefore it appears that a fully frozen PCM tank cannot be obtained during just one night-time of charging the tank (i.e. 12 hours). It seems the preliminary assumed cooling capacity of 2800 kWh per tank cannot be completely utilized during an ordinary operation mode with charging the tank at night and discharging it at daytime. Further investigations in regard of retrieving the complete potential of a PCM storage tank will be discussed in chapter 4.3.3, where an operation mode with an extended melting section will be evaluated.

Figure 32 shows the advantage of modelling the PCM storage. A model provides understanding about the system which is not accessible by measurements under normal circumstances. With varying the discretization of the modelled tank with $n_{cells,flow\ channel}$ along the tank and $n_{cells,PCM}$ into the perpendicular direction, it is possible to make assumptions on the three-dimensional freezing and melting progresses inside the tank.

In figure 32, the rather imbalanced values for the liquid mass fraction in the beginning of the simulation are the result of improper initialization of the PCM tank. Since initialization has a huge effect on the simulation results, the following chapter will focus on this topic.

4.3.2 Measurement 30.05. – 01.06.2016 (3 sections)

In this chapter mostly the same measurement data is used as above. However, the first part of the measurement data, i.e. the daytime of May 30th, is cut out such that the data set starts at 22:00 on May 30th. That way the simulation begins from a different starting point which requires a different initialization. The impact of the changed initialization on the subsequent sections of the PCM storage behaviour can be investigated.

The measurement data and simulation results for this period are presented in figures 33 – 35. Furthermore figure 36 presents the integrated values for the heat transfer rate at the end point of the measurement period. The sections 1 – 3 in figure 34 are equal to the sections 2 – 4 in figure 29. For the last freezing section the model predicts the same trajectory for the outlet temperature as previously. However, the model's estimations for the other two sections are dependent on the initial parametrization of the PCM Tank.

The results for the figures 33 – 36 have been taken from a simulation that was initialized with a partially frozen PCM tank. The discretization was set to $n_{cells,flow\ channel}$ = 3 and $n_{cells,PCM}$ = 2. As for the initial liquid mass fraction, $x_{init,PCM}$ was set to 0.95 and $x_{init,flow\ channel}$ was chosen in a way to decrease the initial liquid mass fraction by 0.2 for each discretized cell in the direction of the flow channel.

As a result of the initially frozen PCM the predicted outlet temperature in figure 34 is slightly lower than the measured one. Though, the trajectory for the estimated outlet temperature in section 2 is more satisfying than in the previous chapter. The model still fails to reproduce the correct overall slope for the outlet temperature trajectory, but the yellow blocks in figure 36 illustrate that the difference in the integrated value of the heat transfer rate has highly decreased for this section (measured 1538.9 kWh, predicted 1668.6 kWh) in comparison to the previous chapter 4.3.1 (measured 1536.3 kWh, predicted 1269.0 kWh). It is self-evident that the integrated value of the predicted heat transfer rate in section 1 is now diverging from the integrated value for the measured heat transfer rate in figure 36. This is because of the new initialization that assumed a partially frozen PCM for the start, leading to a predicted outlet temperature that is lower than the measured outlet temperature in section 1 (figure 34). The initialization of the model has a huge impact not only on the very beginning of the simulation, but also for the subsequent sections as it was shown in this chapter.

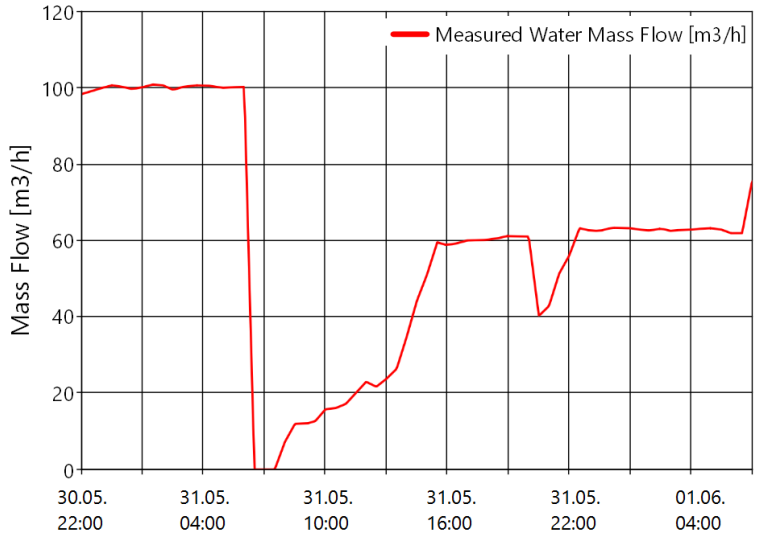

Figure 33 – Measurement 30.05.-01.06.2016 (3 sections, initial x < 1), water mass flow rate in m^3/h

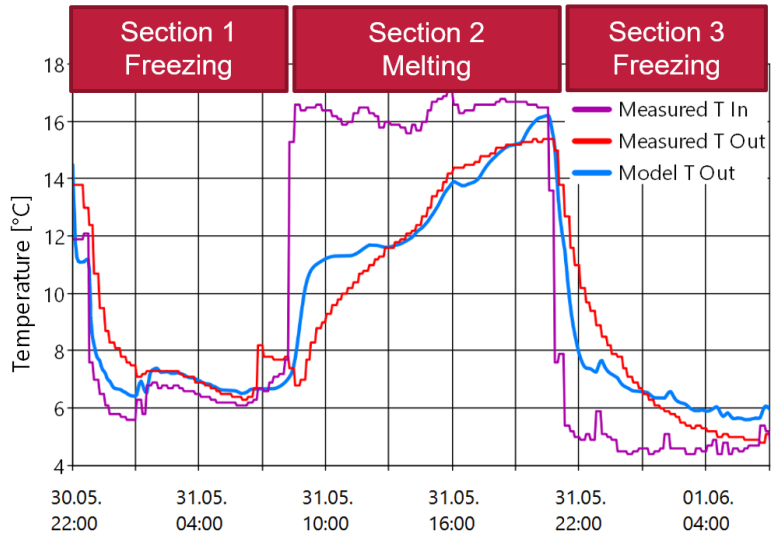

Figure 34 – Measurement 30.05.-01.06.2016 (3 sections, initial x < 1), water inlet + outlet temperature in °C

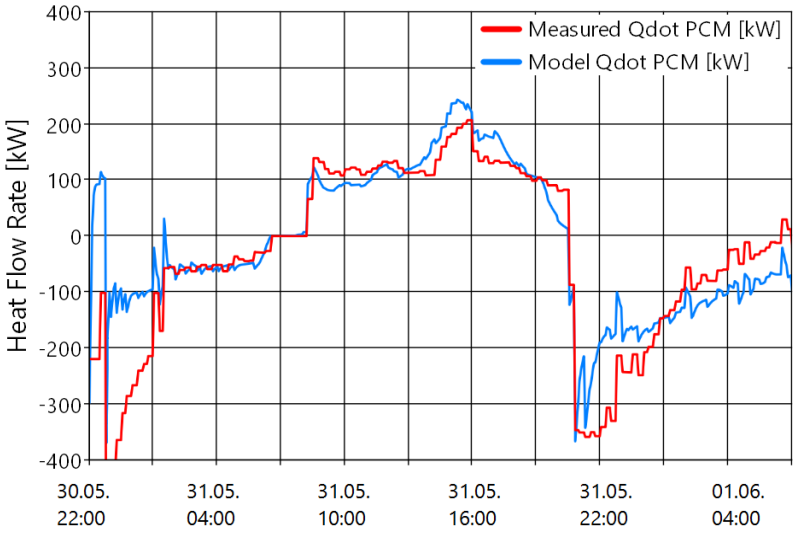

Figure 35 – Measurement 30.05.-01.06.2016 (3 sections, initial x < 1), heat transfer rate of the PCM in kW

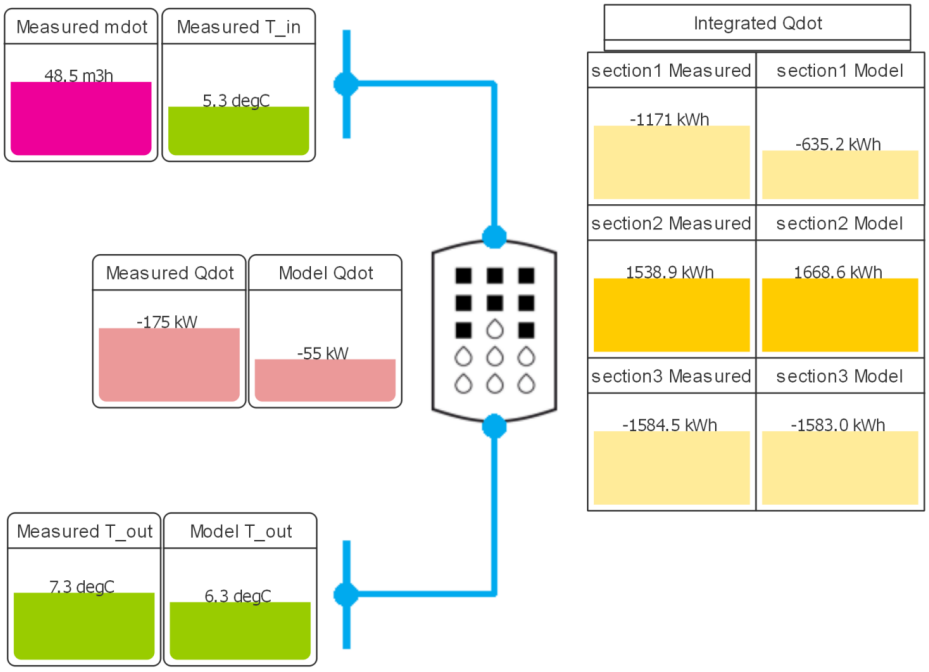

Figure 36 – Simulation end results for measurement 30.05.-01.06.2016 (3 sections, initial x < 1)

For the sake of completeness figures 37 and 38 show the results of the simulation with an initial liquid mass fraction of x_{init} = 1 (fully molten) for every PCM cell. The results are extremely close to the results from the 4-sectional measurement data in the previous chapter 4.3.1 (figures 29 and 31).

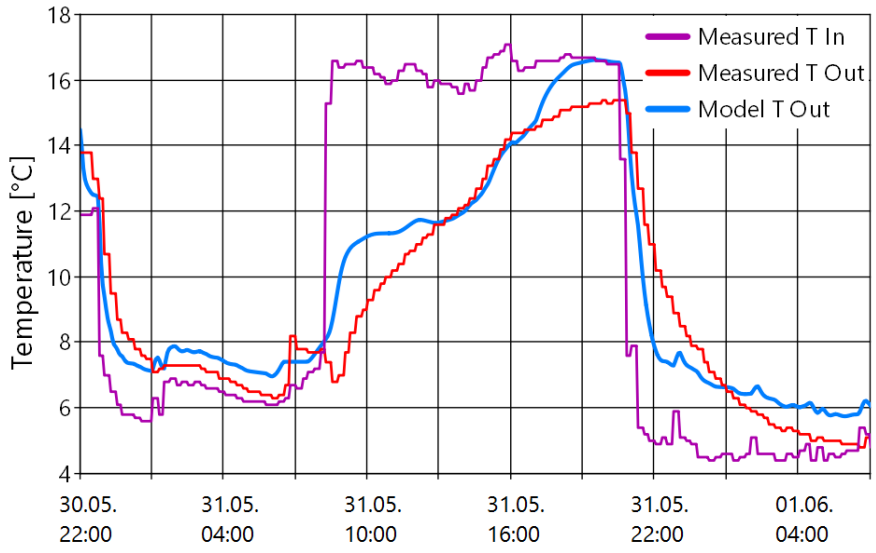

Figure 37 – Measurement 30.05.-01.06.2016 (3 sections, initial x = 1), water inlet + outlet temperature in °C

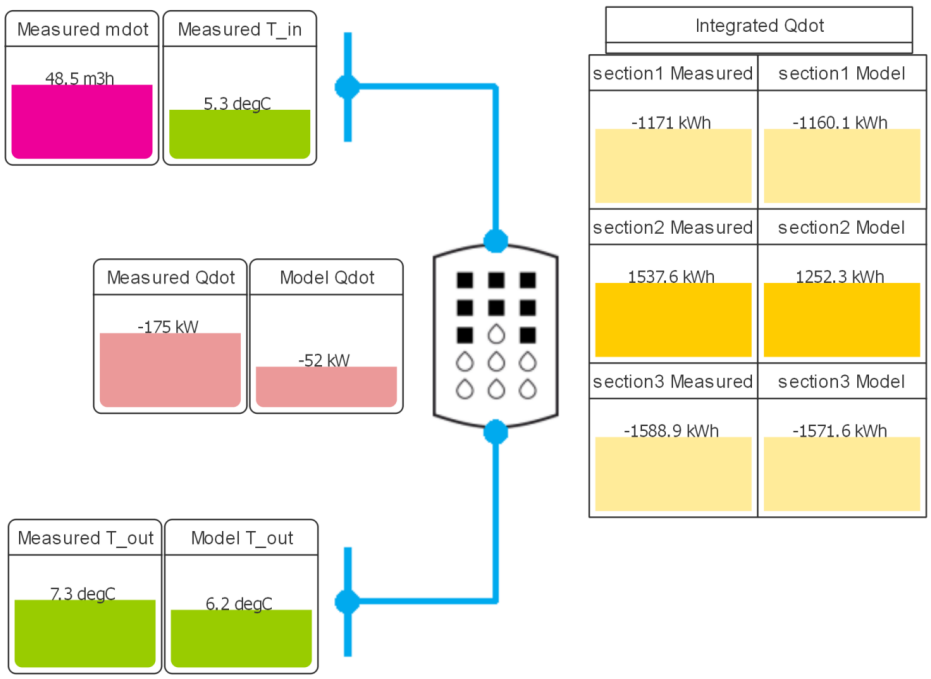

Figure 38 – Simulation end results for measurement 30.05.-01.06.2016 (3 sections, initial x = 1)

This measurement data set from 30.05. – 01.06.2015 was conducted with only PCM tank #1 in use. In the following chapter, the same procedure will be conducted for a different PCM tank.

4.3.3 Measurement 02.06. – 05.06.2016

Analogous to the previous chapter, this measurement data set focuses on the performance of a single PCM tank. During the recorded time period, only PCM tank #3 was supplied with water while the remaining tanks were shut down.

In the investigated period the measured mass flow rate was always higher than zero and varied between 10 – 60 m^3/h.

The freezing and thus charging sections start at 02.06. 21:00 and at 04.06. 19:00, respectively. They last during the whole night-time until the next morning. The melting and thus discharging section is starting at 03.06. 09:00. It lasts over two days and one night until the beginning of the second night. The measured and simulated data for the mass flow rate, inlet and outlet temperatures and heat flow rate are shown in figures 39, 40 and 41, respectively.

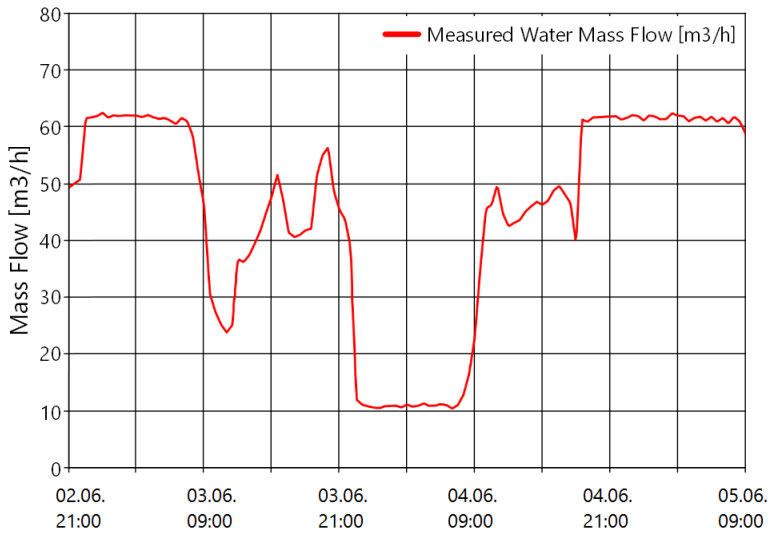

Figure 39 – Measurement 02.06.-05.06.2016, water mass flow rate in m^3/h

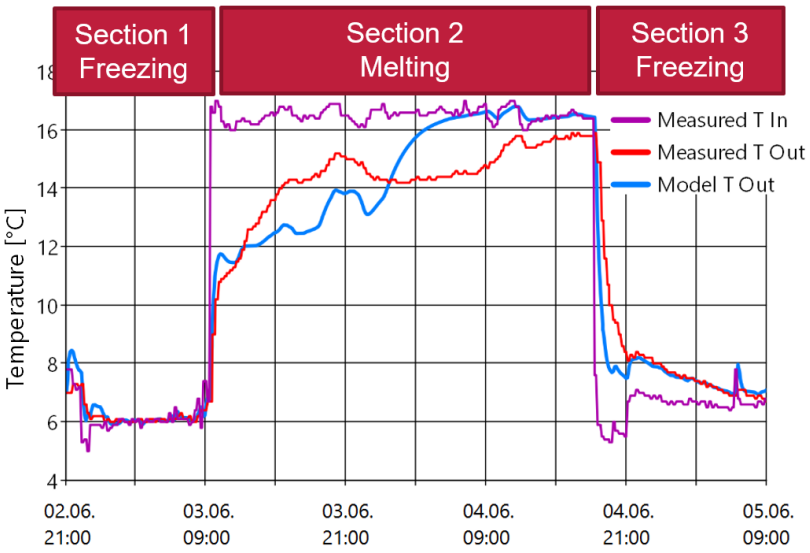

Figure 40 – Measurement 02.06.-05.06.2016, water inlet and outlet temperature in °C

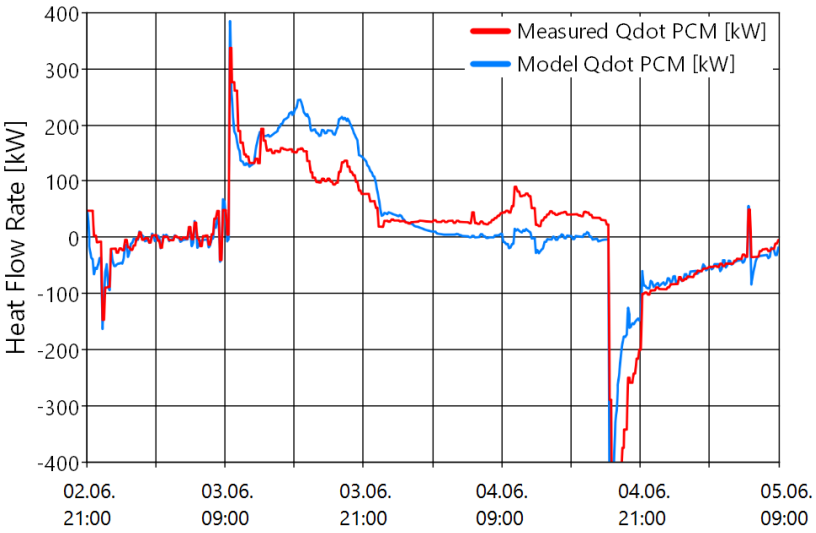

Figure 41 – Measurement 02.06.-05.06.2016, heat transfer rate of the PCM in kW

In general the same conclusions for the predicted outlet temperature can be drawn like in the chapters before: The quality of the prediction of the outlet temperature is better for the freezing sections. In the first half of the melting section the estimated outlet temperature is clearly lower than the measured outlet temperature (figure 40). In the second half of the melting section it is the opposite, and almost equal to the inlet temperature. However, figure 42 (as well as figure 67 in the appendix) show that the model is actually predicting the correct value for the integrated heat transfer for the melting section (measured 2525.4 kWh, predicted 2751.1 kWh). This means, that the model is capable of estimating the correct amount of energy the PCM tank is absorbing during this section. Though, the calculations for the corresponding heat transfer and thus for the temperature trajectory lack refinement and need to be improved for the melting progress in particular, as it was already mentioned in the previous chapters before.

In general, the measurement during the extended melting section demonstrate some effects that require more detailed evaluation. The melting section can be roughly divided into 3 sub-sections, which are differing in their respective mass flow rates: The first sub-section starts at 03.06. 09:00 and lasts 12 hours over the daytime. The mass flow rate during this sub-section is 25 – 50 m^3/h (figure 39) and the heat flow rate is 100 – 150 kWh (figure 41), which resembles the values for the 12-hour-melting sections from the measurement of 30.05.2016 in chapter 4.3.1.

The second sub-section starts at 03.06. 21:00 and lasts 12 hours over the night-time. The mass flow rate is reduced to 10 m^3/h during this time. As a result, the heat transfer rate decreases to 30 kW.

In the last sub-section, which starts at 04.06. 09:00, the mass low rate is increasing again to 40 – 50 m^3/h. However, the correspondent heat transfer rate remains on the low level of approximately 30 – 50 kW (with a transient peak of 90 kW). A reason for this might be the decreased difference between the inlet water temperature and the PCM temperature after 24 hours of melting. Figure 40 shows that the temperature difference between inlet and outlet water temperature has decreased to $< 2\ K$ by then. Thus, the increase of the mass flow rate by the factor of 5 at the end of the melting section at 04.06. 09:00 is needed to compensate the decreasing temperature difference, resulting in a nevertheless constant heat transfer rate in comparison to the previous sub-section.

As a result for the extended melting section that lasted 36 hours, figure 42 illustrates that a total amount of absorbed energy by the PCM of 2525 kWh was achieved. This value resembles the initial design parameter for the PCM tank of 2800 kWh (see chapter 2.2) and implies that the PCM tank appears to be able to utilize its total storage potential in this case, because of the highly extended melting period in combination with an increased mass flow rate at the very end of the melting section. Therefore, as discussed in chapter 4.3.1, the system is not capable of utilizing the complete tank potential during ordinary operation modes that require a charging during the night-time and a discharging during a daytime (i.e. 12 hours for each), as discussed in chapter 2.2. Furthermore, the actual cooling system of the University College of Bergen has implemented four PCM tanks instead of just one. Thus, it appears to be very unlikely that the full PCM storage potential of 11200 kWh could be utilized during ordinary operation modes.

The results in these chapters have shown that both tanks are in principle fully operable. However, the complete potential of the PCM storage tanks cannot be retrieved during a single night-time charging and daytime discharging cycle. Nevertheless, the model managed to reproduce the tank's behaviour with adequate accuracy.

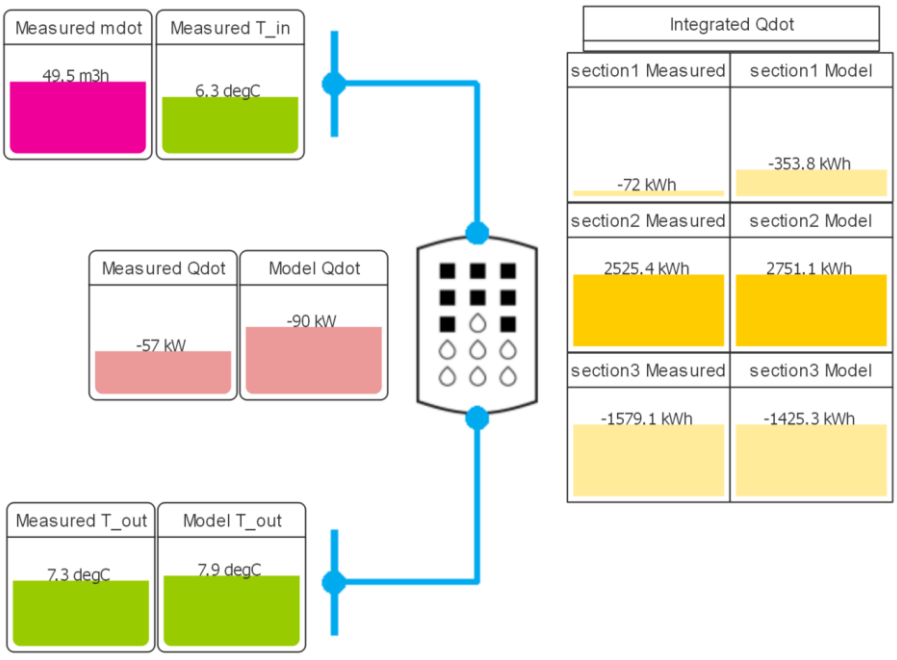

Figure 42 – Simulation end results for measurement 02.06.-05.06.2016

5 Conclusion and Proposal for Further Work

A Modelica based model for simulating the performance of a PCM thermal energy storage has been derived based on a PCM storage unit at the University College of Bergen. The validation of the model was conducted using measurement data from the plant at Bergen. The aim with the model was to provide understanding about the PCM storage behaviour and charging dynamics, and to improve the dimensioning of such storage systems and the design of the operation modes.

It was shown that the measured performance of the PCM tanks is generally matching the preliminary design parameters. Especially during a measurement period in 2016, the PCM storage has been successfully operated with charging and discharging cycles. It was shown that the maximum amount of cooling capacity of 2800 kWh promised by the manufacturer could be reached with the PCM tank, when the melting time is sufficiently long. However, the PCM tank's complete storage potential of 11200 kWh cannot be retrieved during ordinary night-time/daytime charging/discharging cycles. The preliminary design of the storage system appears to be oversized for the University College of Bergen for the present mode of operation. Further research needs to be performed whether the heat transfer rate during ordinary 12 hour charging sections could be enhanced to increase the amount of retrieved storage potential.

The model was capable of predicting the measured values correctly with adequate quality. Especially the values for the amount of absorbed or released energy by the PCM storage were on a satisfying level. However, the correct trend of the trajectory for the outlet temperature still lacks refinement.

The current deviations in the simulation results with respect to the measurement data can be related to the assumptions that were made while deriving the present model. More research needs to be conducted in expressing the influence of the phase change on the heat transfer process. The process of how the heat transfer coefficient is changing with progressing melting or freezing activities within the PCM containers needs to be reproduced in a more accurate way by implementing proper equations and correlations.

In particular, the effect of the buoyancy within the PCM containers needs to be considered. As discussed in chapter 3.3.3, the changing buoyancy during a phase change has a huge

impact on the natural convection within the PCM container. For horizontally aligned PCM containers the heat transfer rate on the bottom of a PCM container is hence higher than for the upper side of the PCM container in case of melting.

As mentioned in section 2.1, subcooling occurs during the freezing of PCM. The particular effect of subcooling on the freezing time, on the trajectory of the predicted temperature and on the overall heat transfer rate requires more investigation and a proper implementation in the model.

Irreversibilities, entropy production and second law efficiency during a phase change need to be highlighted. Their effect on retrieving the maximum amount of storage capacity and their impact on the long-term performance of the PCM require more research.

Furthermore, the mass flow rate within the flow channel should be calculated with a more detailed approach which considers the obstacles within the flow channel. The small auxiliary platforms on the surface of the PCM containers are causing local turbulences that affect the local heat transfer coefficient. Local differentiation between laminar and turbulent flow should to be considered as well. The PCM tanks at the University College of Bergen were equipped with flow distributors to ensure an evenly distributed mass flow rate of water. The present model assumes a perfectly distributed mass flow within the tank.

The PCM container walls between the particular PCM containers were neglected. Their effect on the heat transfer needs to be investigated, since the HDPE walls increase the heat resistance for the heat flow within the layer of PCM containers. The tank's steel wall was neglected when estimating the heat capacity of the system. An increased thermal mass is affecting the heat transfer rate especially for the PCM containers close to the tank's wall. Moreover, more detailed material properties for the PCM are lacking for both the liquid and the solid state. Especially for the liquid state the material properties were only approximated with using comparable values from literature.

More precise freezing and melting profiles are needed to validate the model for several boundary conditions, such as varying mass flow rates. Generally, more precise measurement data with a higher quality would greatly help to improve the model.

As for future prospects, assuming that the model accuracy could be successfully increased as discussed above, the model could be used to provide best practise data sheets for future

dimensioning of new plants or for improving the operation of existing ones. Furthermore, the model could be utilized for visualizing and predicting the behaviour of system parameters that cannot be studied by measurements. A system layout as shown in figure 42 or a user interface as shown in figure 43 present possible ways to visualize non-measurable system parameters. That way, accurate information and updated values could be provided for e.g. the distribution of the temperature over the tank or the local liquid mass fraction x for a particular layer of the PCM storage. Such a visualization tool could enable live performance assessment, system debugging, maintenance operation for deficient PCM containers or general prevention of improper operation modes.

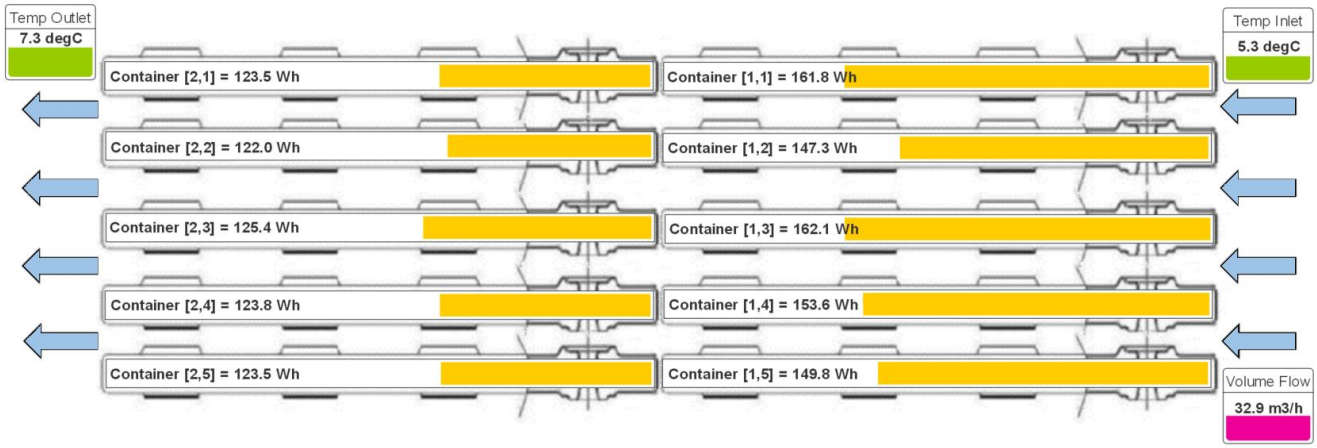

Figure 43 – Future outlook: Potential of live visualization for non-measurable system parameters like the integrated heat transfer rate for each PCM container (side view on the tank's inlet, 2x5 stacked containers with exemplified values)

6 References

Dar, U., 2014. Høgskolen i Bergen Energisentral, SWECO.

Frohböse, I., 2015. TIL Suite Simulates Thermal Systems Software Containing Models for Thermophysical Properties, Thermal Components and Systems, TLK-Thermo GmbH, Braunschweig

Fox, R., et al., 2004. Introduction to Fluid Mechanics, Sixth Edition, Purdue University

Libeer, W., et al., 2016. Two-Phase Heat and Mass Transfer of Phase Change Materials in Thermal Management Systems, Department of Mechanical Engineering, Stanford University

Liu, L., et al., 2016. Thermal Conductivity Enhancement of Phase Change Materials for Thermal Energy Storage: A Review, School of Physics, Nanjing University

Kalnæs, S., Jelle, B., Phase Change Materials and Products for Building Applications: A State-of-the-Art Review and Future Research Opportunities, Department of Civil and Transport Engineering, Norwegian University of Science and Technology (NTNU)

Mehling, H., Cabeza, L.F., 2008. Heat and Cold Storage with PCM: An up-to-date Introduction into Basics and Applications, Springer, ISBN 978-3-540-68557-9

PCM Products Ltd., 2011. PlusICE Phase Change Materials, http://www.pcmproducts.net/files/thermal_storage_catalogue.pdf, retrieved 26.07.2016

PCM Products Ltd., 2011. Thermal Energy Storage Design Guide http://www.pcmproducts.net/files/design_manual.pdf, retrieved 26.07.2016

Perez-Lombard, L., Ortiz, J., Pout, C., A Review on Buildings Energy Consumption Information, Energy and Buildings 40 (3) (2008) 394–398

Sharma, A., et al., 2007. Review on Thermal Energy Storage with Phase Change Materials and Applications, Department of Mechanical Engineering, Kun Shan University

Stene, J.,2014. Heating/Cooling of Academy Buildings. The University of Bergen – New Buildings/Renovation

Sun, X., et al., 2015. Experimental Observations on the Heat Transfer Enhancement Caused by Natural Convection during Melting of Solid–Liquid Phase Change Materials, School of Energy and Power Engineering, Changsha University of Science and Technology

Sweco, 2014. Høgskole i Bergen Funksjonsbeskrivelse, SWECO

Uno, 2007. Housing, Energy and Thermal Comfort: A review. http://www.euro.who.int/__data/assets/pdf_file/0008/97091/E89887.pdf, retrieved 26.07.

Ure, Z., 2008. Thermal Storage, http://www.pcmproducts.net/files/TES-2008.pdf, retrieved 26.07.2016

VDI Heat Atlas, 2013. 11th Edition, Verein Deutscher Ingenieure, VDI-Gesellschaft Verfahrenstechnik und Chemieingenieurwesen (GVC)

A Appendix – Additional Results

A.1 Measurement Data 21.06. – 23.06.2015

Given below are the integrated heat transfer rates $\int \dot{Q}$ for each section as a function of time for the measurement period of 21.06. – 23.06.2016, discussed in section 4.2.2, figure 27.

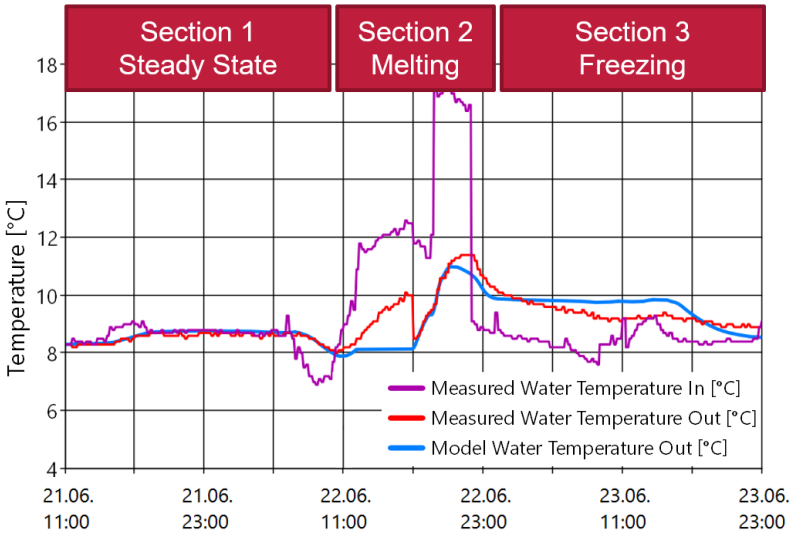

Figure 44 – Measurement 21.-23.06.2015, definition of the sections

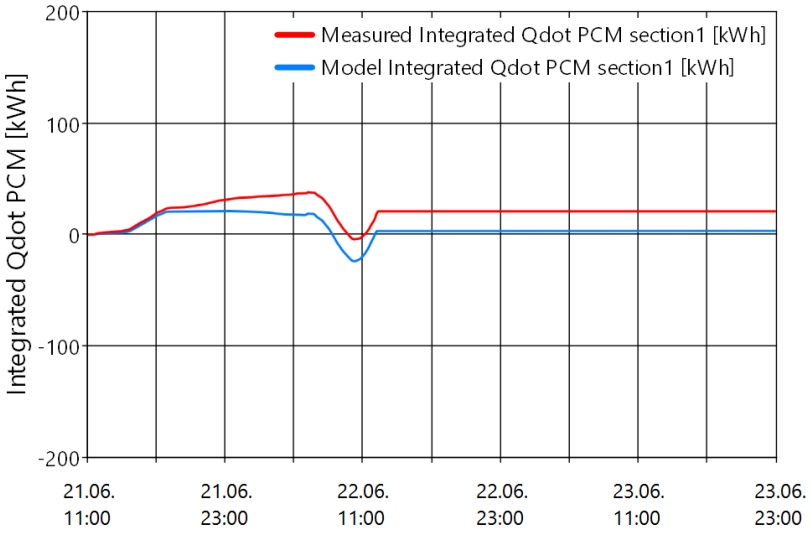

Figure 45 – Measurement 21.-23.06.2015, integrated heat transfer rate section 1 in kWh

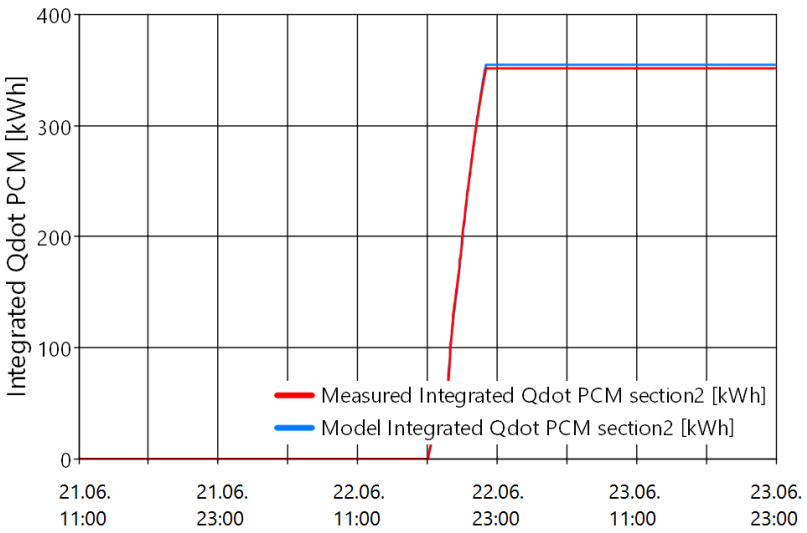

Figure 46 – Measurement 21.-23.06.2015, integrated heat transfer rate section 2 in kWh

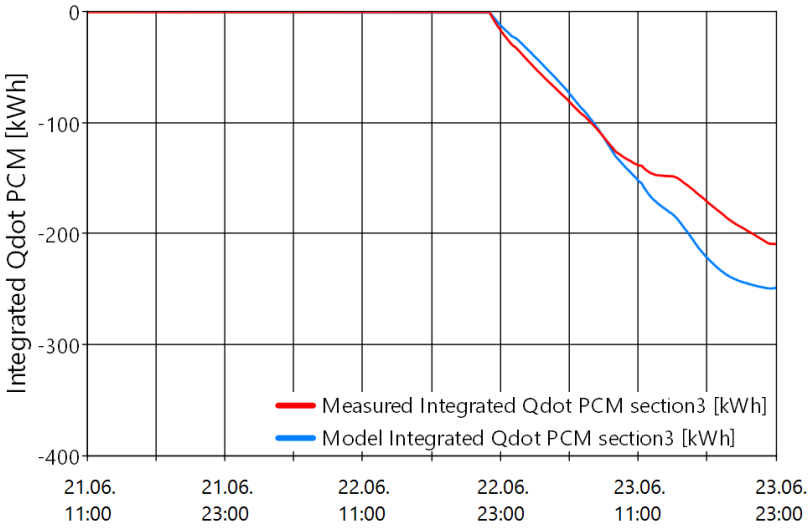

Figure 47 – Measurement 21.-23.06.2015, integrated heat transfer rate section 3 in kWh

A.2 Measurement Data 29.06. – 06.07.2015

The figures 48 – 50 are illustrating the measurement data and the simulation results for the week from June 29th until July 6th 2015 during normal operation of the building, where typical low cooling demand conditions occur. Among other things, the measured values for the heat transfer seem to be improper, since a non-zero heat transfer is measured despite equal inlet and outlet temperatures. Therefore it was decided to not further utilize any data from this week for the sake of validation in the report.

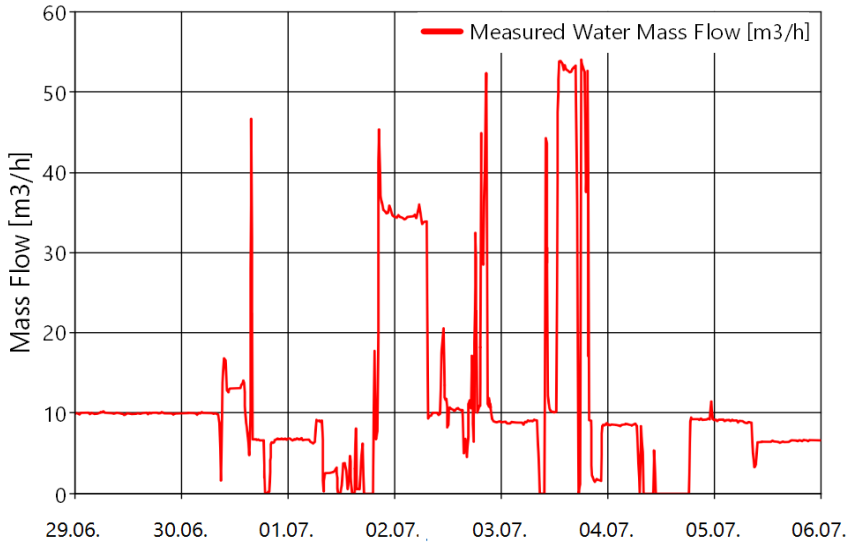

Figure 48 – Measurement 29.06.-06.07.2015, water mass flow rate in m^3/h

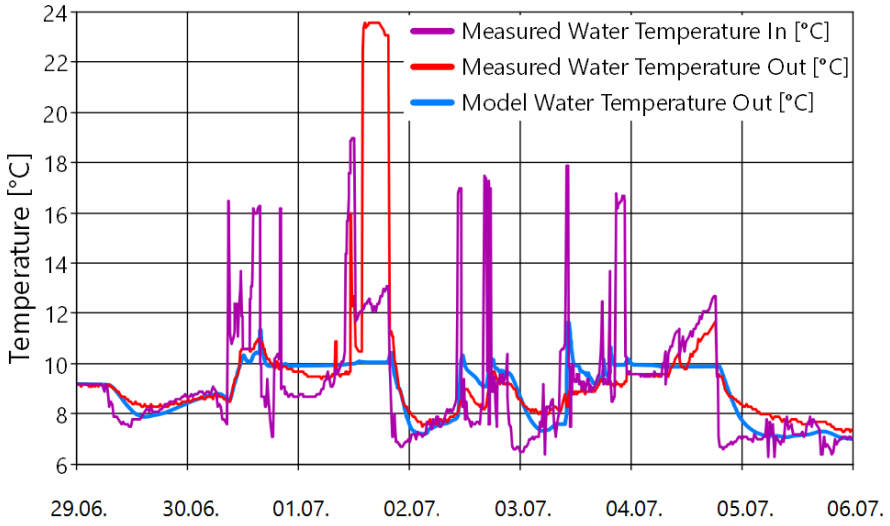

Figure 49 – Measurement 29.06.-06.07.2015, water inlet and outlet temperature in ℃

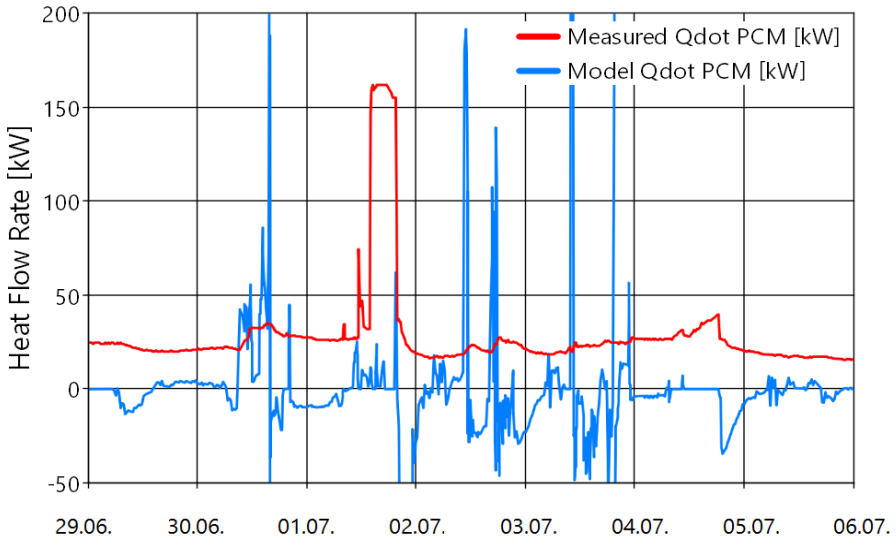

Figure 50 – Measurement 29.06.-06.07.2015, heat transfer rate of the PCM in kW

A.3 Measurement Data 01.06. – 26.07.2015

For a roundup of the measurement data set from 2015 the results of the simulation of the overall two month time period is given in figures 51 – 55. The most important tendencies of the model's behaviour towards the 2015-measurement have been elaborated in chapter 4.2 of the report. Some improper peaks or major deviations of the measured values in the following figures might result from measurement inaccuracies or general system errors and are hence not discussed further.

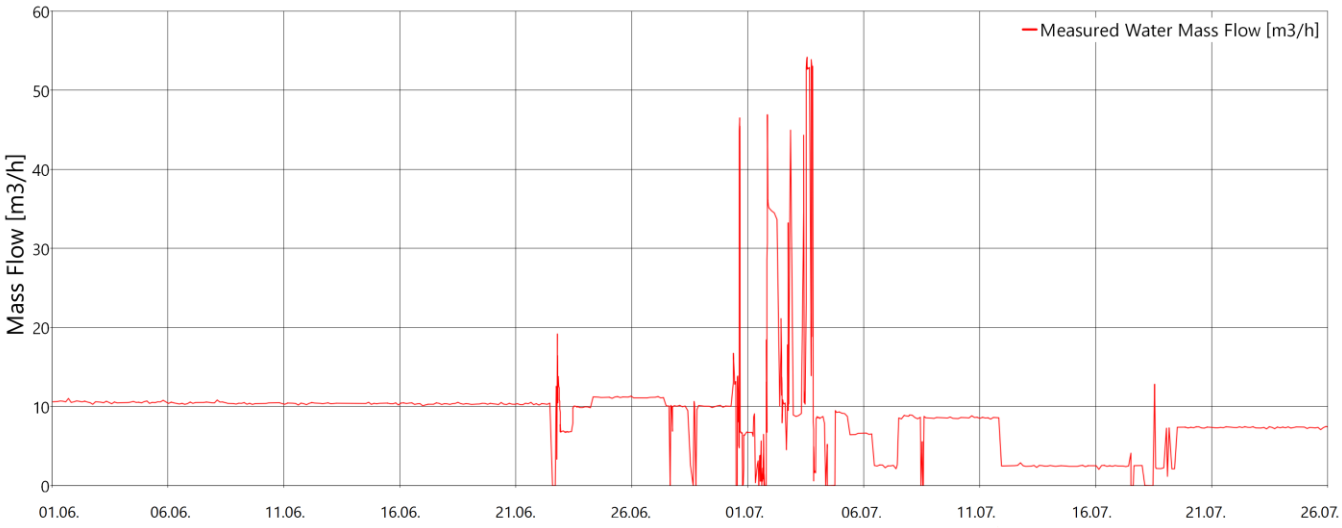

Figure 51 – Measurement 01.06. – 26.07.2015, measured water mass flow rate in m^3/h

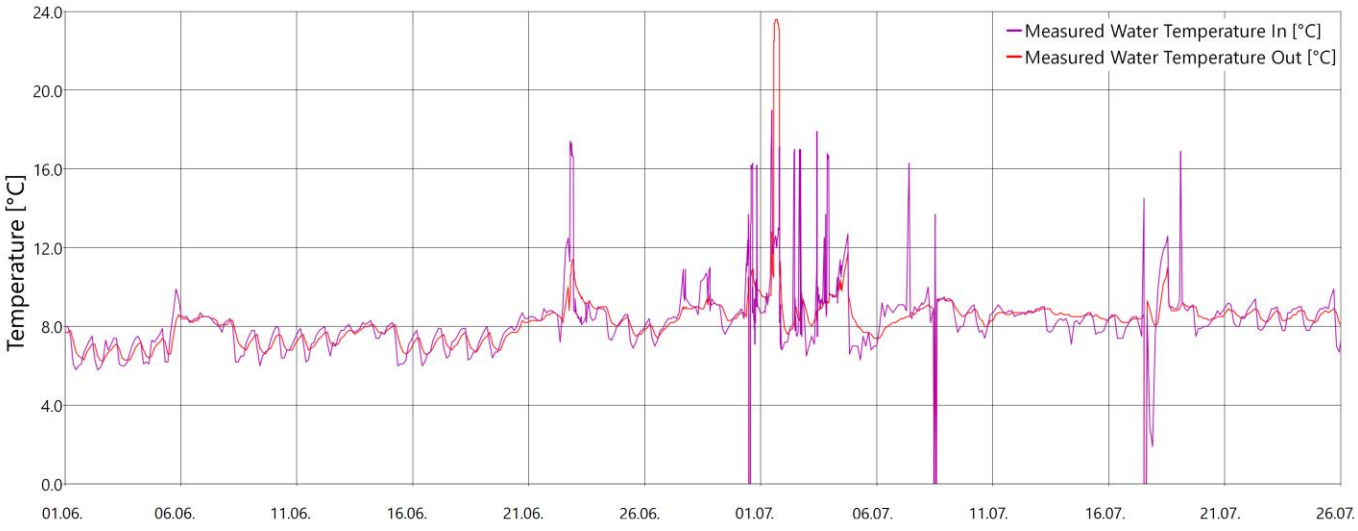

Figure 52 – Measurement 01.06. – 26.07.2015, measured inlet and outlet water temperature in $°C$

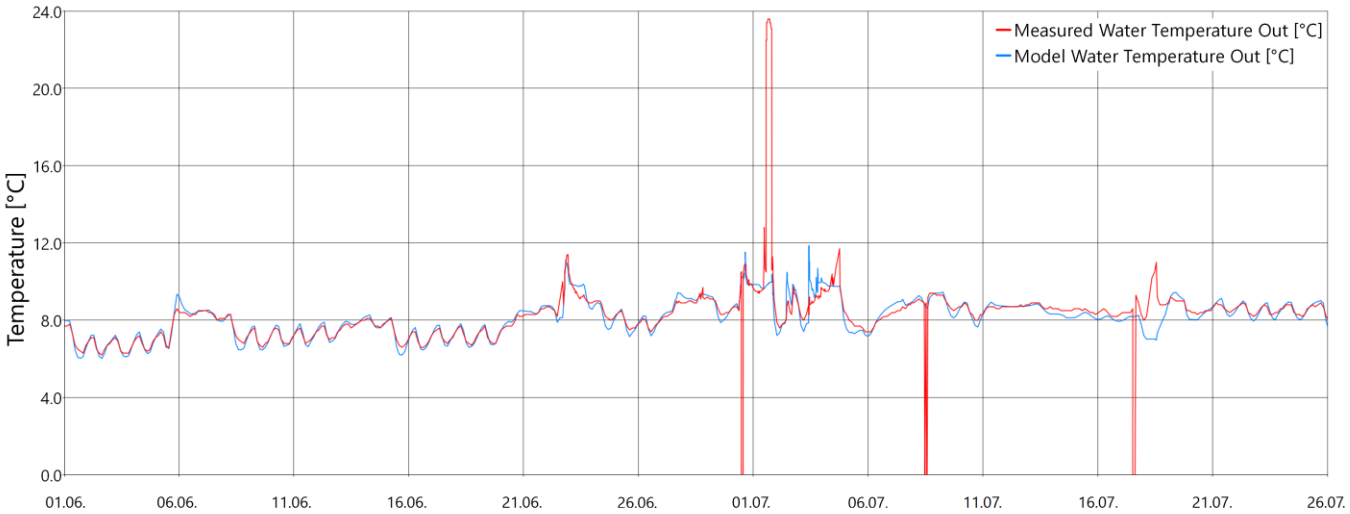

Figure 53 – Measurement 01.06. – 26.07.2015, measured and predicted outlet water temperature in °C

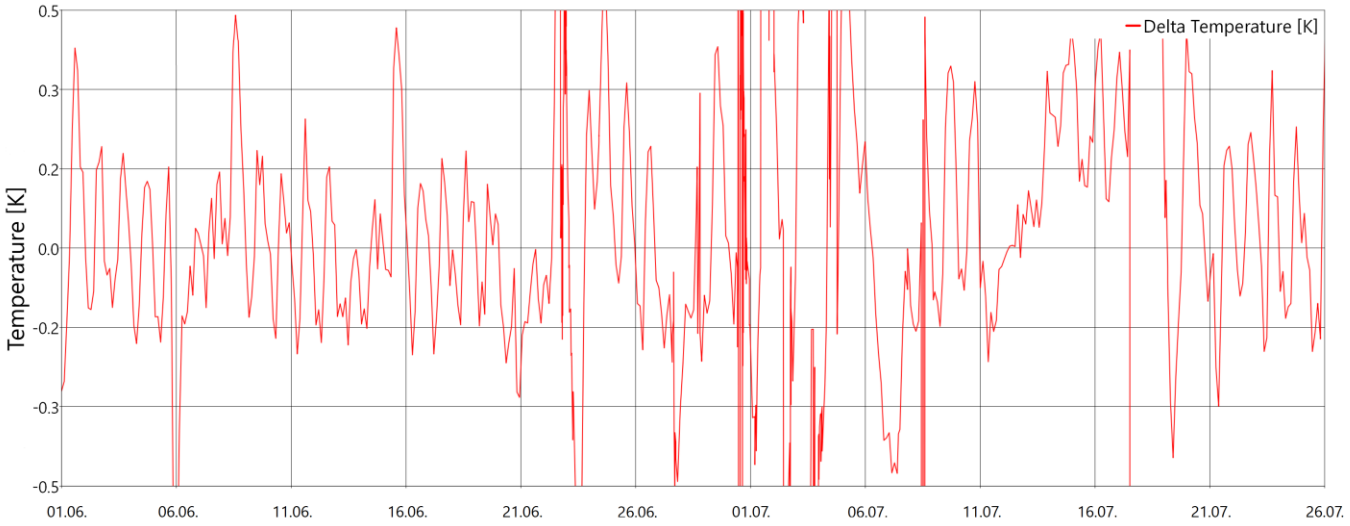

Figure 54 – Measurement 01.06. – 26.07.2015, difference of measured and predicted outlet temperature in °C

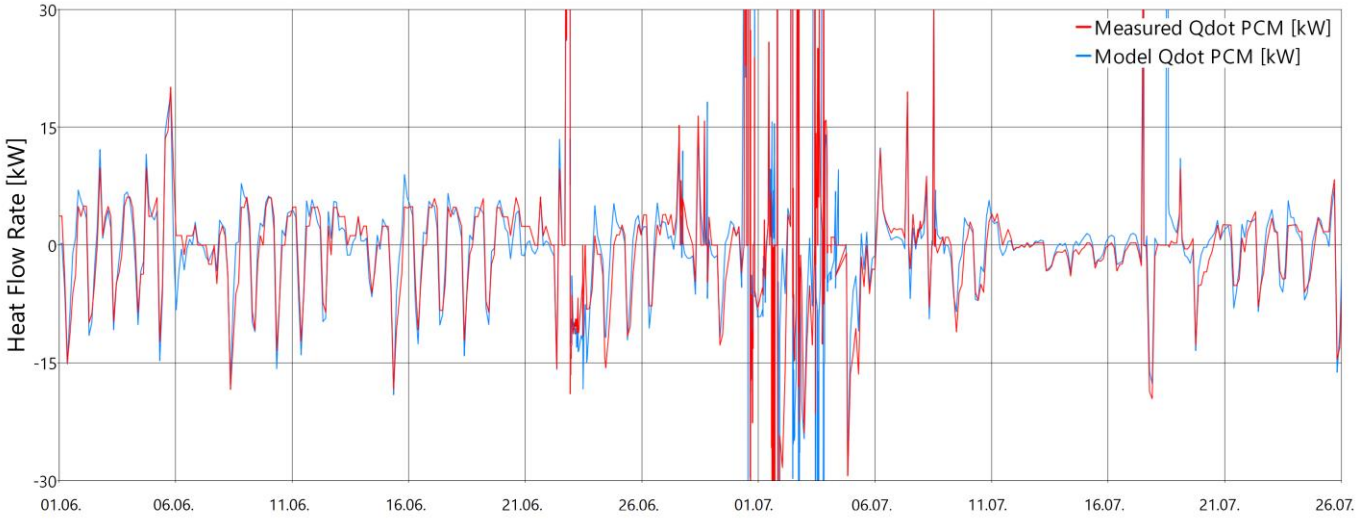

Figure 55 – Measurement 01.06. – 26.07.2015, measured and predicted heat transfer rate in kW

A.4 Measurement Data 30.05. – 01.06.2016 (4 sections)

Given below are the integrated heat transfer rates $\int \dot{Q}$ for each section as a function of time for the measurement period of 30.05. – 01.06.2016, discussed in section 4.3.1, figure 31.

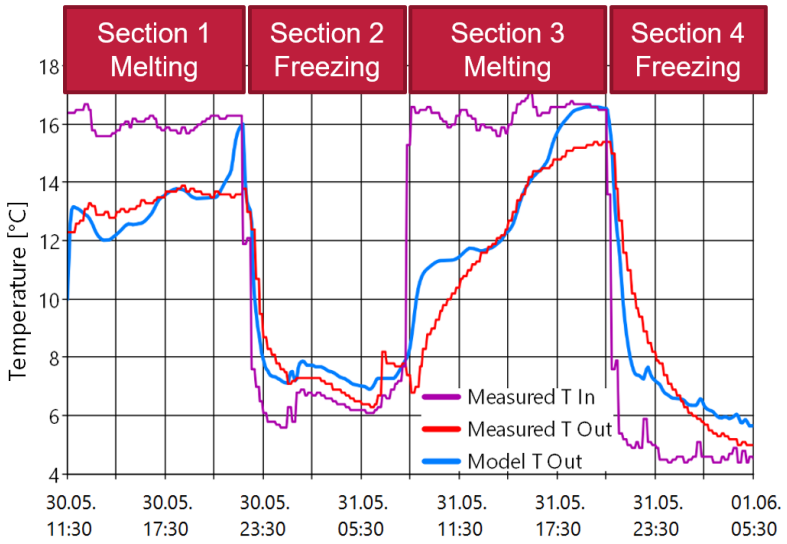

Figure 56 – Measurement 30.05.-01.06.2016 (4 sections), definition of the sections

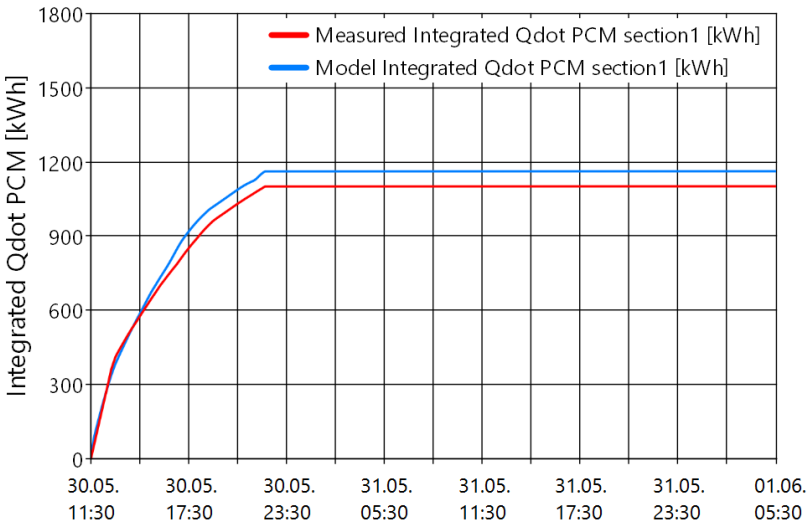

Figure 57 – Measurement 30.05.-01.06.2016 (4 sections), integrated heat transfer rate section 1 in kWh

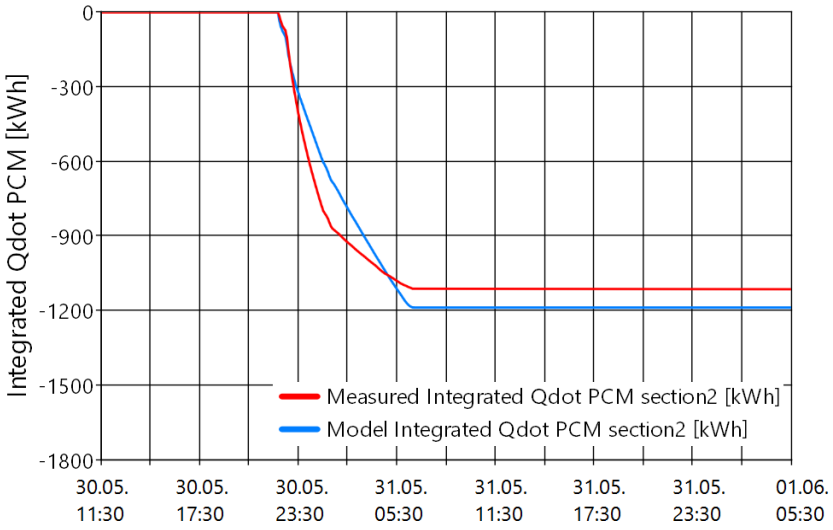

Figure 58 – Measurement 30.05.-01.06.2016 (4 sections), integrated heat transfer rate section 2 in kWh

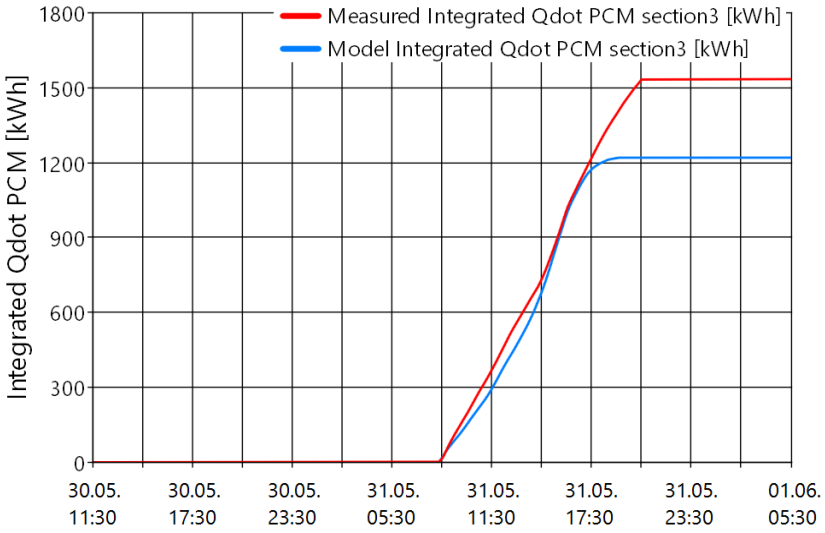

Figure 59 – Measurement 30.05.-01.06.2016 (4 sections), integrated heat transfer rate section 3 in kWh

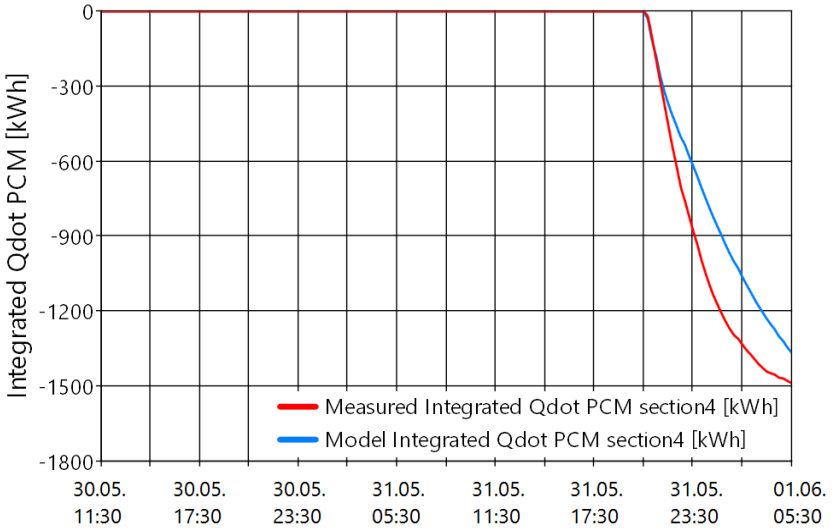

Figure 60 – Measurement 30.05.-01.06.2016 (4 sections), integrated heat transfer rate section 4 in kWh

A.5 Measurement Data 30.05. – 01.06.2016 (3 sections)

Given below are the integrated heat transfer rates $\int \dot{Q}$ for each section as a function of time for the measurement period of 30.05. – 01.06.2016, discussed in section 4.3.2, figure 36.

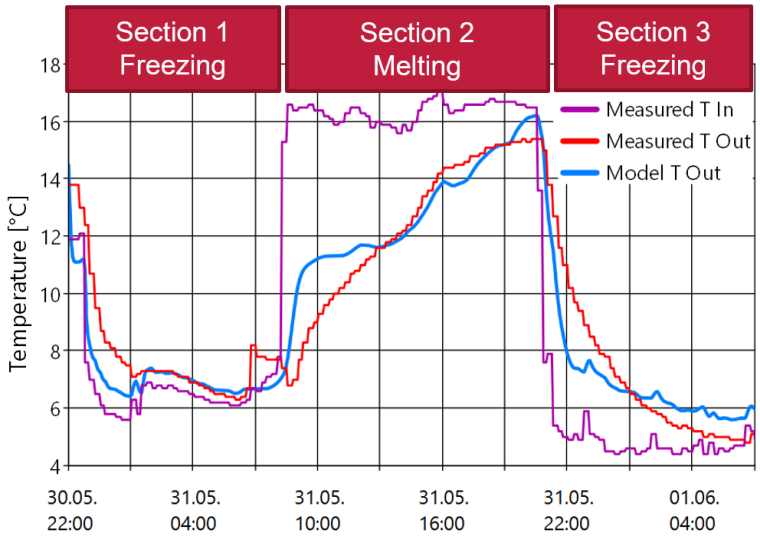

Figure 61 – Measurement 30.05.-01.06.2016 (3 sections), definition of the sections

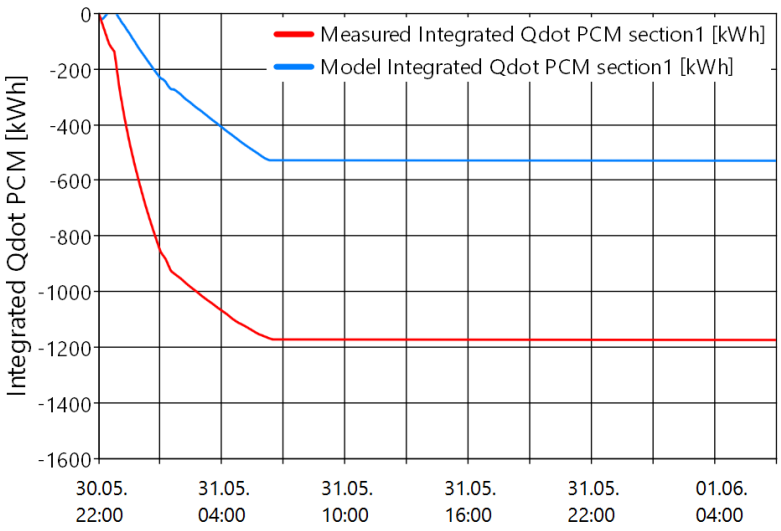

Figure 62 – Measurement 30.05.-01.06.2016 (3 sections), integrated heat transfer rate section 1 in kWh

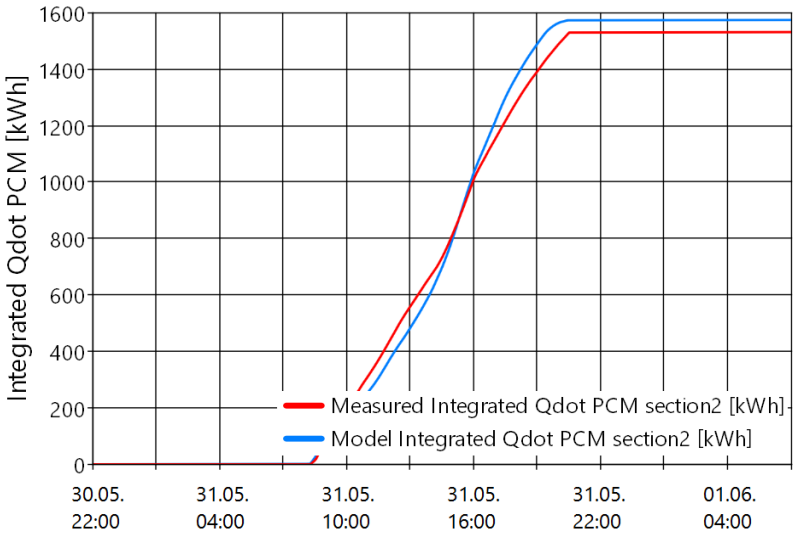

Figure 63 – Measurement 30.05.-01.06.2016 (3 sections), integrated heat transfer rate section 2 in kWh

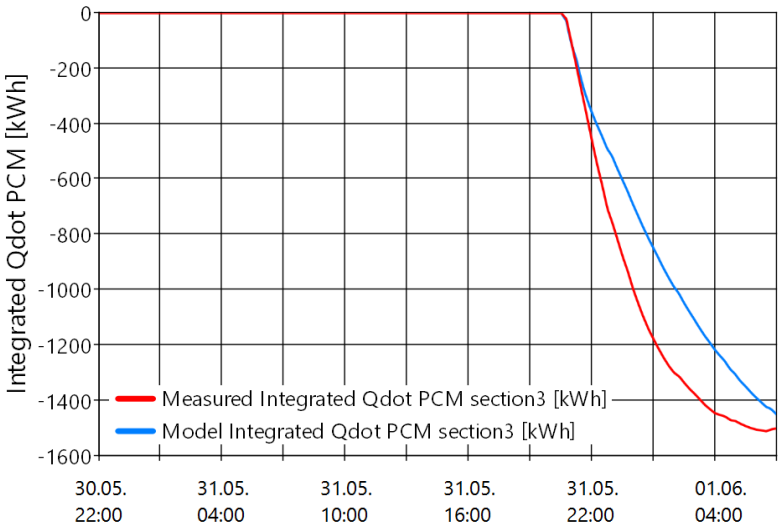

Figure 64 – Measurement 30.05.-01.06.2016 (3 sections), integrated heat transfer rate section 3 in kWh

A.6 Measurement Data 02.06. – 05.06.2016

Given below are the integrated heat transfer rates $\int \dot{Q}$ for each section as a function of time for the measurement period of 02.06. – 05.06.2016, discussed in section 4.3.3, figure 42.

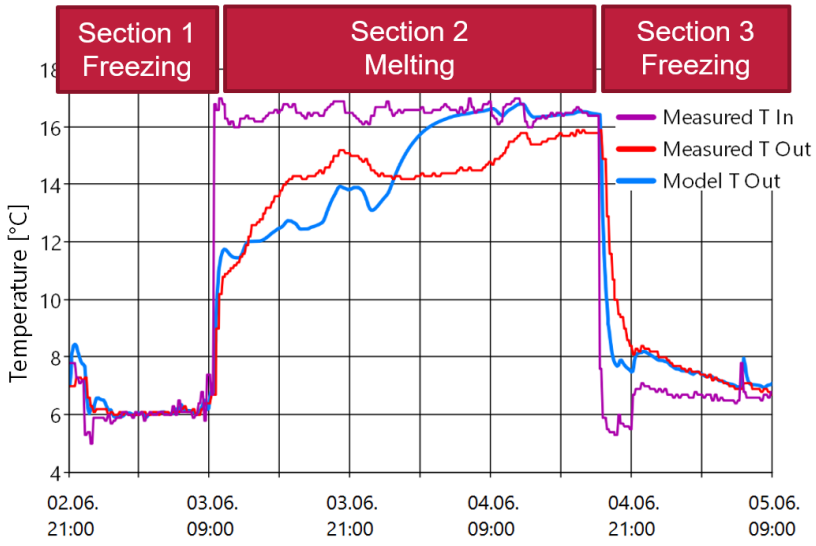

Figure 65 – Measurement 02.06.-05.06.2016, definition of the sections

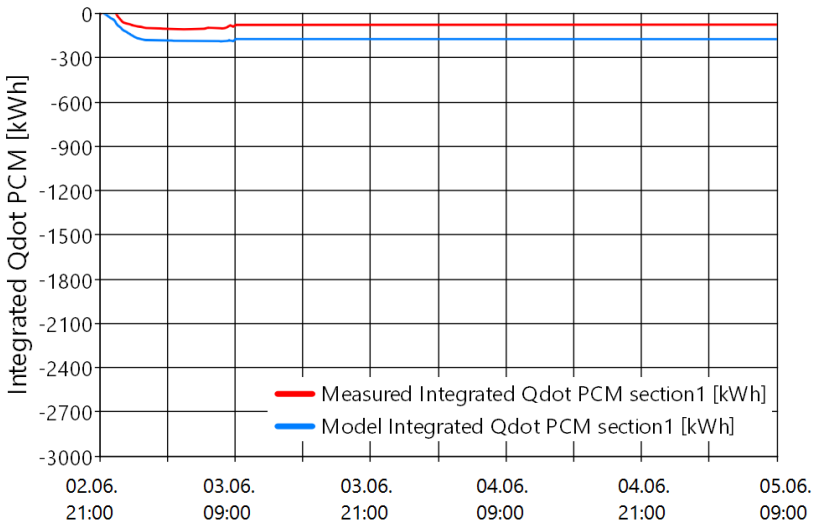

Figure 66 – Measurement 02.06.-05.06.2016, integrated heat transfer rate section 1 in kWh

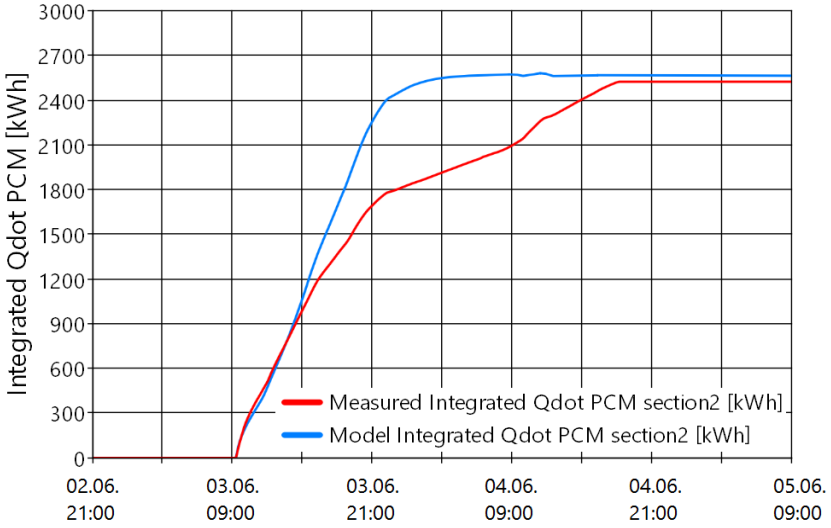

Figure 67 – Measurement 02.06.-05.06.2016, integrated heat transfer rate section 2 in kWh

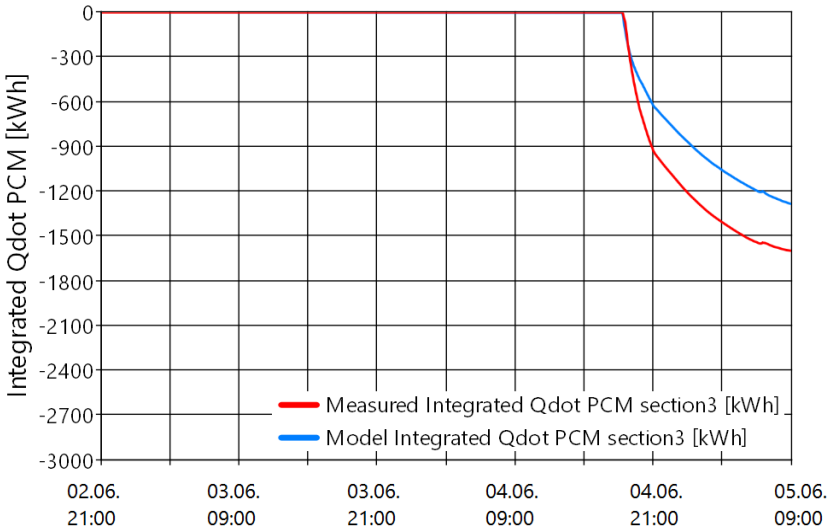

Figure 68 – Measurement 02.06.-05.06.2016, integrated heat transfer rate section 3 in kWh

A.7 Comparison of Approaches for Heat Transfer Coefficient Estimation

Chapter 3.3 discussed the different approaches for calculating the heat transfer coefficient on the liquid side of the PCM heat exchanger model. Literature provides several possible cases that can be utilized when modelling a PCM storage (VDI Heat Atlas 2013). The validation proved that the best simulation results were obtained when assuming the case "flow over a horizontal plane". The results for this particular approach of estimating the heat transfer coefficient were discussed in detail in chapter 4.

The second possible case for calculating the heat transfer coefficient for the PCM heat exchanger model is "flow in a flat gap between two heated walls". The heat transfer coefficient becomes (VDI Heat Atlas 2013):

$$\alpha_{water} = \frac{k_{freeze\ time} * \lambda * Nu}{2 * h_{flow\ channel}} \tag{23}$$

With a Nusselt number of

$$Nu = 7.55 + \left(\frac{0.024 * \left(\frac{Re * Pr * 2 * h_{flow\ channel}}{l_{flow\ channel}}\right)^{1.14}}{1 + 0.0358 * \left(\frac{Re * Pr * 2 * h_{flow\ channel}}{l_{flow\ channel}}\right)^{0.64} * Pr^{0.17}}\right) \tag{24}$$

This equation is valid for laminar flows. There is no need for considering a turbulent Nusselt number calculation in this particular case, since the Reynolds number is now:

$$Re = \frac{2 * h_{flow\ channel} * v * \rho}{\eta} \tag{25}$$

This case utilizes a different approach to estimate the flow characteristics for the heat transfer. Thus, the Reynolds number is a function of the channel height and not a function of the channel length as in the case before (equation 11). Hence, the Reynolds number remains $<$ (1^5) for all measured volume flows in chapter 4 and no turbulent flow occurs.

The equation for the flow velocity remains the same (see equation 12).

For the sake of comparison, figures 69 – 71 show the simulation results for the case "flow in a flat gap between two heated walls" for the same measurement data set from 30.05. – 01.06.2016 that was already used in chapter 4.3.1.

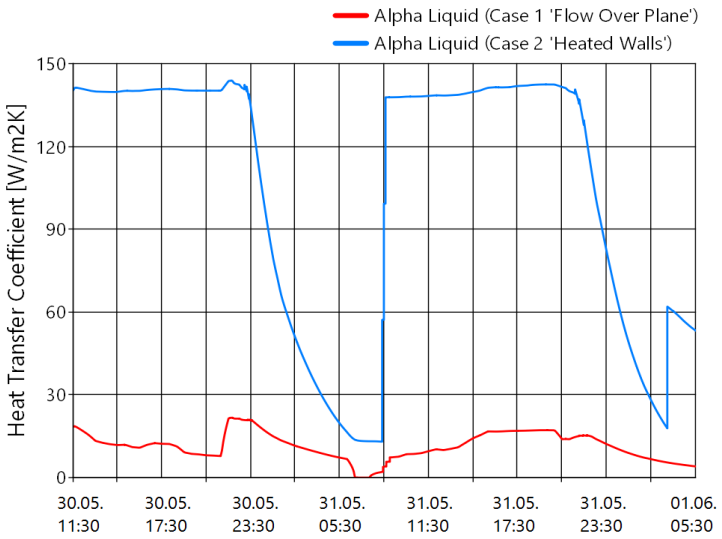

Figure 69 – Comparison of approaches for alpha estimation, heat transfer coefficient alpha in W/m^2K for case 1 "flow over plane" and case 2 "heated walls"

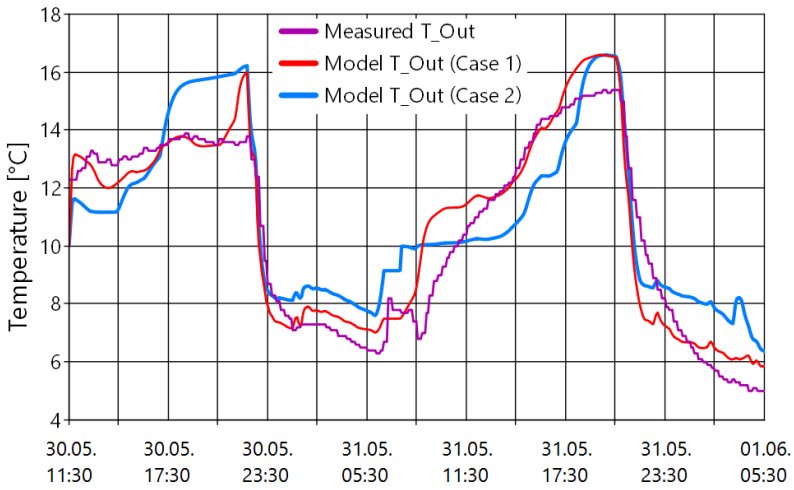

Figure 70 – Comparison of approaches for alpha estimation, water inlet and outlet temperature in °C for case 1 "flow over plane" and case 2 "heated walls"

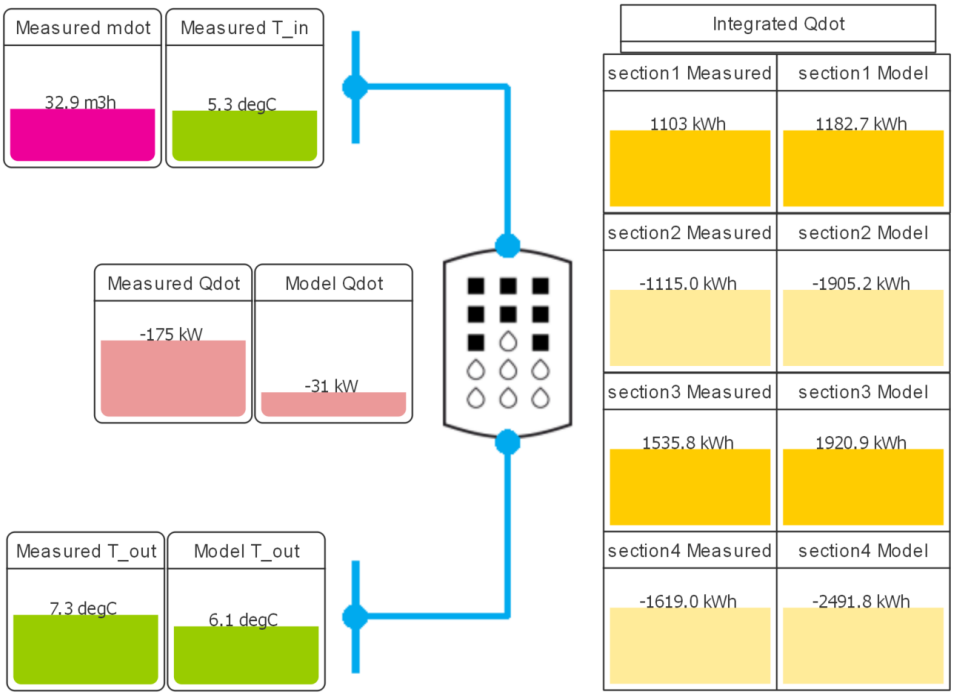

Figure 71 – Simulation end results for measurement 30.05.-01.06.2015, heat transfer coefficient estimated applying the case "heated walls"

As shown on figure 69, the calculated heat transfer coefficient is higher by the factor of 10 for the case 2 "flow in a flat gap between two heated walls". The average heat transfer coefficient is 15 $\frac{W}{m^2K}$ for case 1 and 140 $\frac{W}{m^2K}$ for case 2. As a result, the trajectory of the predicted outlet temperature is fluctuating more (figure 70) than the trajectory that was estimated with applying case 1 "flow over a horizontal plane" in figure 29. Furthermore the deviations of the integrated values for the heat transfer rate between the measured and predicted values in figure 71 are higher than the values in chapter 4.3.1 as well.

Thus, for this case even more modifying factors like the freezing time factor $k_{freeze\ time}$ from chapter 3.3 are required to tune the equations and to shape the progress of the heat transfer towards the measured values. For the present time, the simulation results from chapter 4 that were estimated with applying the case 1, proved quite satisfying quality with comparatively little effort in modifying these factors. Thus, it was decided to continue working with applying the case of "flow over a horizontal plane".

However, a future outlook might be to further investigate the performance of the system when case 2 is applied or even to derivate a completely new case that fits the PCM heat exchanger model the best, since it was shown that the calculation of the heat transfer coefficient has a high impact on the overall performance of the PCM storage model.